



National Library
of Canada

Bibliothèque nationale
du Canada

Canadian Theses Service

Service des thèses canadiennes

Ottawa, Canada
K1A 0N4

NOTICE

The quality of this microform is heavily dependent upon the quality of the original thesis submitted for microfilming. Every effort has been made to ensure the highest quality of reproduction possible.

If pages are missing, contact the university which granted the degree.

Some pages may have indistinct print especially if the original pages were typed with a poor typewriter ribbon or if the university sent us an inferior photocopy.

Previously copyrighted materials (journal articles, published tests, etc.) are not filmed.

Reproduction in full or in part of this microform is governed by the Canadian Copyright Act, R.S.C. 1970, c. C-30.

AVIS

La qualité de cette microforme dépend grandement de la qualité de la thèse soumise au microfilmage. Nous avons tout fait pour assurer une qualité supérieure de reproduction.

S'il manque des pages, veuillez communiquer avec l'université qui a conféré le grade.

La qualité d'impression de certaines pages peut laisser à désirer, surtout si les pages originales ont été dactylographiées à l'aide d'un ruban usé ou si l'université nous a fait parvenir une photocopie de qualité inférieure.

Les documents qui font déjà l'objet d'un droit d'auteur (articles de revue, tests publiés, etc.) ne sont pas microfilmés.

La reproduction, même partielle, de cette microforme est soumise à la Loi canadienne sur le droit d'auteur, SRC 1970, c. C-30.

THE UNIVERSITY OF ALBERTA

BEAM-FOIL STUDY OF ARVI

by



ZONGQIANG GE

A THESIS

SUBMITTED TO THE FACULTY OF GRADUATE STUDIES AND RESEARCH
IN PARTIAL FULFILMENT OF THE REQUIREMENTS FOR THE DEGREE
OF MASTER OF SCIENCE

DEPARTMENT OF PHYSICS

EDMONTON, ALBERTA

SPRING 1988

Permission has been granted to the National Library of Canada to microfilm this thesis and to lend or sell copies of the film.

The author (copyright owner) has reserved other publication rights, and neither the thesis nor extensive extracts from it may be printed or otherwise reproduced without his/her written permission.

L'autorisation a été accordée à la Bibliothèque nationale du Canada de microfilmer cette thèse et de prêter ou de vendre des exemplaires du film.

L'auteur (titulaire du droit d'auteur) se réserve les autres droits de publication; ni la thèse ni de longs extraits de celle-ci ne doivent être imprimés ou autrement reproduits sans son autorisation écrite.

ISBN 0-315-42808-2

THE UNIVERSITY OF ALBERTA

RELEASE FORM

NAME OF AUTHOR

ZONGQIANG GE

TITLE OF THESIS

BEAM-FOIL STUDY OF ARVI

DEGREE FOR WHICH THESIS WAS PRESENTED MASTER OF SCIENCE

YEAR THIS DEGREE GRANTED SPRING 1988

Permission is hereby granted to THE UNIVERSITY OF ALBERTA LIBRARY to reproduce single copies of this thesis and to lend or sell such copies for private, scholarly or scientific research purposes only.

The author reserves other publication rights, and neither the thesis nor extensive extracts from it may be printed or otherwise reproduced without the author's written permission.

(SIGNED) *Ge, Zongqiang*

PERMANENT ADDRESS:

*HANGZHOU INSTITUTE OF
ELECTRONIC ENGINEERING
CHINA*

DATED *April 26* 1988

THE UNIVERSITY OF ALBERTA
FACULTY OF GRADUATE STUDIES AND RESEARCH

The undersigned certify that they have read, and recommend to the Faculty of Graduate Studies and Research, for acceptance, a thesis entitled BEAM-FOIL STUDY OF ARVI submitted by ZONGQIANG GE in partial fulfilment of the requirements for the degree of MASTER OF SCIENCE in PHYSICS.

F. J. Finnington

Supervisor

W. B. Oliver
J. A. Kopylov
W. H. ...

Date. *March 28, 1988...*

ABSTRACT

The ArVI spectrum has been investigated by the methods of beam-foil spectroscopy. An analysis of the spectra obtained at 1.6 MeV is used to suggest new assignments for levels of the $3p^2$ and $3s3p3d$ electron configurations. Decay curves for transitions from these levels have been recorded and yield lifetimes that are typically almost 30% longer than the values calculated by Fawcett. Various analyses, including the ANDC technique, incorporating the transitions from $3p^2$ and $3s3p3d$ levels, are also employed to estimate the lifetimes of the resonance doublet levels. The results from the ANDC method are generally in good agreement with Fawcett's calculations for the $3s3p^2$ 2S , 2P , 2D and $3s^23d$ 2D levels, although the uncertainty in the $3s3p^2$ 2P ($J=3/2$) result is relatively large. A comparison of the observed level energies and lifetimes with the calculation by Fawcett shows excellent consistency with a recent study of the isoelectronic ion, TiX.

ACKNOWLEDGEMENT

I am grateful to my supervisor, Dr. E.H. Pinnington for his inspiring motivating guidance and most valuable assistance throughout this project.

I wish to thank Dr. J.A. Kernahan for his valuable assistance during the experiments and for providing results of decay curve analyses using the FORTRAN routine, DISCRETE.

Dr. W. Ansbacher has been responsible for many significant improvements in experimental techniques, which proved to be very beneficial in this project. I much appreciate his making available a new computer program, ANDC. His assistance during the project is also appreciated.

Mr. R.N. Gosselin has been responsible in designing and improving an ANDC routine named ANDC.LINE. I am appreciative of his valuable work.

I also wish to thank Dr. J.P. Buchet and Dr. A.E. Livingston, for offering their BFS spectra at the higher energies, and Messrs. R. Gardner and L. Coulson, for their operation of the 2MV accelerator. Finally, I wish to thank the UNIVERSITY OF ALBERTA for financial support during the period of this project.

Table of Contents

Chapter	Page
1. INTRODUCTION	1
2. DATA ACQUISITION	7
2.1 Experimental Arrangement	7
2.2 Spectrum Recording	11
2.3 Intensity Decay Curve Recording	12
3. SPECTROSCOPIC ANALYSIS	17
3.1 All Isoelectronic Sequence Trends	17
3.2 Energy Dependence of Spectral Line Intensity	19
3.3 Computer Spectral Analysis	27
3.4 Level Confirmation by Decay Curve Comparison	28
3.5 Assignment for the $3p^3$ and $3s3p3d$ levels	30
3.5.1 $3p^3$ Levels	30
3.5.2 $3s3p(^3P)3d$ Levels	31
3.5.3 $3s3p(^1P)3d$ Levels	33
3.5.4 Summary of the Spectroscopic Assignments	40
4. TECHNIQUES FOR DECAY CURVE ANALYSIS	45
4.1 Multi-Exponential Curve-Fitting Techniques	45
4.2 The ANDC Technique	47
4.3 The VNET Technique	50
5. LIFETIME MEASUREMENTS	58
5.1 Lifetimes of Levels of the $3p^3$ and $3s3p3d$ Configuration	58
5.2 Lifetimes of the $3s3p^3$ and $3s^23d$ Energy Levels	59
5.2.1 $3s3p^3 \ ^3S$	61
5.2.2 $3s3p^3 \ ^3P$	62
5.2.3 $3s3p^3 \ ^3D$	63

5.2.4 $3s^23d\ ^2D$	63
5.3 Discussion of Lifetime Results	63
6. SUMMARY AND CONCLUSIONS	68
BIBLIOGRAPHY	72
APPENDIX I SURVEY SPECTRUM	75
APPENDIX II COMPUTER ROUTINE USED IN SPECTRAL ANALYSIS ...	80
APPENDIX III DETAILS OF TFIT ANALYSIS	82
APPENDIX IV THEORETICAL ESTIMATES FOR LIFETIMES OF CASCADE LEVELS	86
APPENDIX V SAMPLE LIFETIME ANALYSES	90

LIST OF TABLES

TABLE

PAGE

3.1	Suggested Assignments for Some ArVI Transition	42
3.2	Suggested Energy Level Assignments for ArVI	44
5.1	Radiative Lifetimes of $3p^2$ and $3s3p3d$ Levels of ArVI	60
5.2	Radiative Lifetimes of $3s3p^2$ and $3s^23d$ Levels of ArVI	66
5.3	Comparison with Previous Experiments	67
6.1	Comparison with Theoretical Calculations	71
A4.1	Theoretical Calculation of A-values and Lifetimes for $3p^2$ and $3s3p3d$ Levels	87

LIST OF FIGURES

FIGURE	PAGE
2.1 Sketch of the Data Acquisition System	9
2.2 Detection System Geometry	15
3.1 Isoelectronic Sequence Trends for the $3p^1$ and $3s3p(^1P)3d^1P, ^1D$ Terms	20
3.2 Isoelectronic Sequence Trends for the $3s3p(^1P)3d^1F$ and $3s3p(^1P)3d^1D$ Terms	22
3.3 Energy Dependence of the Ar Charge State Distribution.....	25
3.4 Beam-Foil Spectrum of Ar around 619A	35
3.5 Beam-Foil Spectrum of Ar around 783A	35
3.6 Beam-Foil Spectrum of Ar around 509A	37
3.7 Beam-Foil Spectrum of Ar from 468 to 488A	37
4.1 Representative Energy Level Scheme	51
4.2 Schematic Decay Curve Used in an ANDC Analysis	53
A1.1 Survey Spectra	76
A4.1 Energy Level Scheme of ArVI ($n=3$)	88
A5.1 Sample Lifetime Analyses	92

1. INTRODUCTION

Since the pioneer work by Kay (Ka63) and Bashkin (Ba64), beam-foil spectroscopy (BFS) has proved to be a powerful method for obtaining atomic lifetimes and spectra. The basic principle of this technique is quite straightforward. A fast ion beam (usually produced by an accelerator) is further ionized by a thin foil. The foil (usually carbon of order 1000A in thickness) defines a localized excitation region. This is especially important in the measurement of short lifetimes. The second advantage of the foil excitation mechanism is its efficient production of multiply-ionized atoms. In principle, all ionic species of the beam atoms can be obtained, and therefore the beam foil source is spectroscopically very rich. The fact that a range of ionized atoms can be found in foil-excited beams implies that very many excited electronic states within these ions can be produced. Theoretically, almost any excited level of any ionic state of a given atom can be studied using this technique, providing that the appropriate accelerating potential is used. The price paid for the non-selective nature of this excitation is possible line-blending, and hence difficulty in spectral identification, as well as the complication of cascade repopulation in lifetime measurements. Since the First International Conference on Beam-Foil Spectroscopy in 1967, hundreds of papers have been published in this field.

The principle of lifetime measurements is quite simple in the case where a single energy level is populated. All the atoms in the beam move with essentially the same velocity. The characteristic spontaneous emission by the foil-excited ions is detected on the downstream side of the foil. The lifetime of a given excited energy level can be obtained by measuring the fluorescent intensity at the wavelength corresponding to a transition from that level as a function of distance along the beam. Thus, if only the single level in question were populated, the intensity would follow the well-known exponential decay. However, the non-selective character of the excitation mechanism causes repopulation by cascades, i.e. the energy level of interest is repopulated by other, more highly excited levels. Therefore the intensity decay curve normally appears as a sum of exponential terms. The technique of multi-exponential (m-e) curve fitting aims to find the best fit of an observed decay curve to such a sum. Since many of the higher electronic states have been excited to some extent, the number of exponential terms could be very large. In practice, the number of exponential terms that can be included in a given fit is relatively small, typically two or three, so that the result of such an analysis must be an approximation. It is therefore important that any such analysis should contain a rigorous treatment of errors that has first been tested using synthetic data.

A more rigorous method of analysis was first suggested by E.J. Curtis and his colleagues in 1970 (CBB70). The principle of this method is to incorporate decay curves from the cascading transitions that repopulate a given level in the analysis of the lifetime of that level. Since it is not necessary that all the decay curves in a given analysis have the same intensity calibration, this method is described as an analysis using Arbitrary Normalized Decay Curves (ANDC). The ANDC method has been used extensively to obtain lifetimes for the resonance lines in atoms where there are one or two active electrons. In one electron systems, such as those belonging to the NaI, CuI and AgI isoelectronic sequences (EEB83, PBK181, KPAB85), the cascades are dominated by the transition from the energy levels in the "yrast" chain. For example, the yrast chain for the resonance line of Na-like atoms has the form as follows: $3p-3d-4f-5g$ Hence the ANDC method is easy to use, as only the single direct cascade ($3p-3d$ in the NaI example) is of major importance in the analysis. For atoms having two active electrons, the decay scheme is still relatively simple. The ANDC method proved to be successful in the Be-like sequence, although no yrast chain exists there. Engström et al. (EDE71) included cascades from three levels ($2p^2$ 'S, 'D and $2s3d$ 'D) into the $2s2p$ 'P level in their ANDC analysis of the $2s2p$ 'P lifetime. The ANDC method was also employed in Zn-like ($n=4$), Cd-like ($n=5$) and Hg-like ($n=6$) atoms (PBK82, BPK82, PAK84, KPAB85, PAK185, OPDB70),

where the in-shell terms (p^2 'S', 'D' and sd 'D') were the most important cascades for sp resonance levels.

The simplest examples of atoms having three active electrons are the B-like atoms ($n=2$). In the study of NIII in 1985 (PAGK86), it was found that the main cascades for the resonance $2s2p^2$ levels are from $2p^3$ and $2s2p3d$ configurations. For Al-like atoms ($n=3$) the in-shell electronic structure is more complicated than for B-like atoms, as there are more in-shell ($\Delta n=0$) cascades for these resonance levels. It can be expected that it is more difficult to use the ANDC analysis to yield accurate lifetimes when more cascades are important. The recent systematic study of TiX (PAHH87) is the first example in discussing the application of the ANDC method in such a case. The main aim of the present work is to provide a further example.

The ions of the AlI isoelectronic sequence have been paid considerable attention recently by theorists (Fi81, Fa83, AUT84, Hu86), as they provide an interesting example of strong configuration-interactions, particularly between the $3p^2$ and $3s3p3d$ configuration. This configuration interaction results in irregularities in f -values of in-shell transitions along the sequence. The experimental evidence is still rather fragmentary, however, and hence a study of ArVI is of some value in testing the calculations. The third reason to study this ion is, of course, to extend the analysis of its spectrum, which is still very

incomplete.

Among the calculations, both Fawcett (Fa83) and Huang (Hu86) give the results for the energies of all $3s^2 3p$, $3s3p^2$, $3p^3$ and $3s3p3d$ levels, as well as estimating the probabilities of the transitions between them for the ions of the AlI isoelectronic sequence. These two calculations yield similar sequence trends and similar gf-values for $(n=3)$ in-shell transitions along this sequence. These results proved very valuable for this work.

Chapter 2 introduces the experimental arrangement for data acquisition. Because many of the energy levels of the $3p^3$ and $3s3p3d$ configurations were unknown for ArVI prior to this work, the assignment of these levels formed the first step in this project. In Chapter 3, estimates for energies of the $3p^3$ and $3s3p3d$ levels were obtained from isoelectronic sequence comparisons. In this procedure, some previously assigned terms are reassigned for low Z members, including ArVI, to give consistency with theoretical calculations. The estimates largely depend on comparing the previously observed values for AlI, SiII, PIII, SiV, ClV and TiX with theoretical calculations. The estimates of the level energies thus derived are then used as a guide in analysis of the observed spectra. From this analysis, 15 levels of $3p^3$ and $3s3p3d$ configurations are suggested based on 30 transitions identified in the spectra. Previous classification of the charged state (where available) and the intensity dependence on ion energy have been considered

6

in the identification of these lines. Other evidence, such as lifetime measurements and comparing the shapes of decay curves measured for different branches from the same upper level, is also included to support these assignments.

Chapter 4 briefly introduces the principles of the various methods for analysis of BFS decay curves used in this project. Chapter 5 summarizes the observed lifetimes from the various analyses discussed in Chapter 4 for all the resonance levels and the newly-assigned cascade levels. The results from the ANDC analysis for the resonance levels are generally in good agreement with the theoretical calculations (Fa83) for the $3s3p^2\ ^1S$, 1P , 1D and $3s^23d\ ^1D$ levels, although the analysis is less satisfactory for the 1P ($J=3/2$) level. Although a systematic discrepancy with theory of almost 30% is found for the observed cascade lifetimes, their relative values are generally in agreement with the theoretical predictions.

Chapter 6 summarizes the procedures used and the main results obtained in this work. These results are compared both with theory and with the recent experiment of the isoelectronic ions, TiX . The TiX and $ArVI$ results show excellent consistency.

2. DATA ACQUISITION

The basic experimental arrangement for beam-foil spectroscopy is well-known. A brief description of the experimental arrangement used in this project will be given in the first section of this chapter. The second and third sections will describe how the spectra and the intensity decay curves were recorded in this project.

2.1 Experimental Arrangement

The 2MV Van de Graaff accelerator, which is situated in the Radiation Laboratory at the University of Alberta and equipped with a conventional radio frequency ion source, was employed to generate a singly-ionized argon beam. Most of work was conducted using an ion energy of 1.64MeV, since this was the maximum energy that gave a strong and stable beam. (The Ar^{2+} component was found to be too weak.) An electromagnet was used to deflect the Ar^+ beam through a horizontal angle of ~ 8 degree. The separation of the magnet and the target chamber was 3 meters (see Fig. 2.1). A limiting aperture (5mm diameter) immediately before the target chamber thus gave a mass resolution of ~ 1 a.m.u. for Ar^+ ions.

Mesh-mounted carbon foils of nominal thickness around $5\mu\text{g}/\text{cm}^2$ were used to further ionize and excite the argon atoms. Since the target foil tends to become thicker under

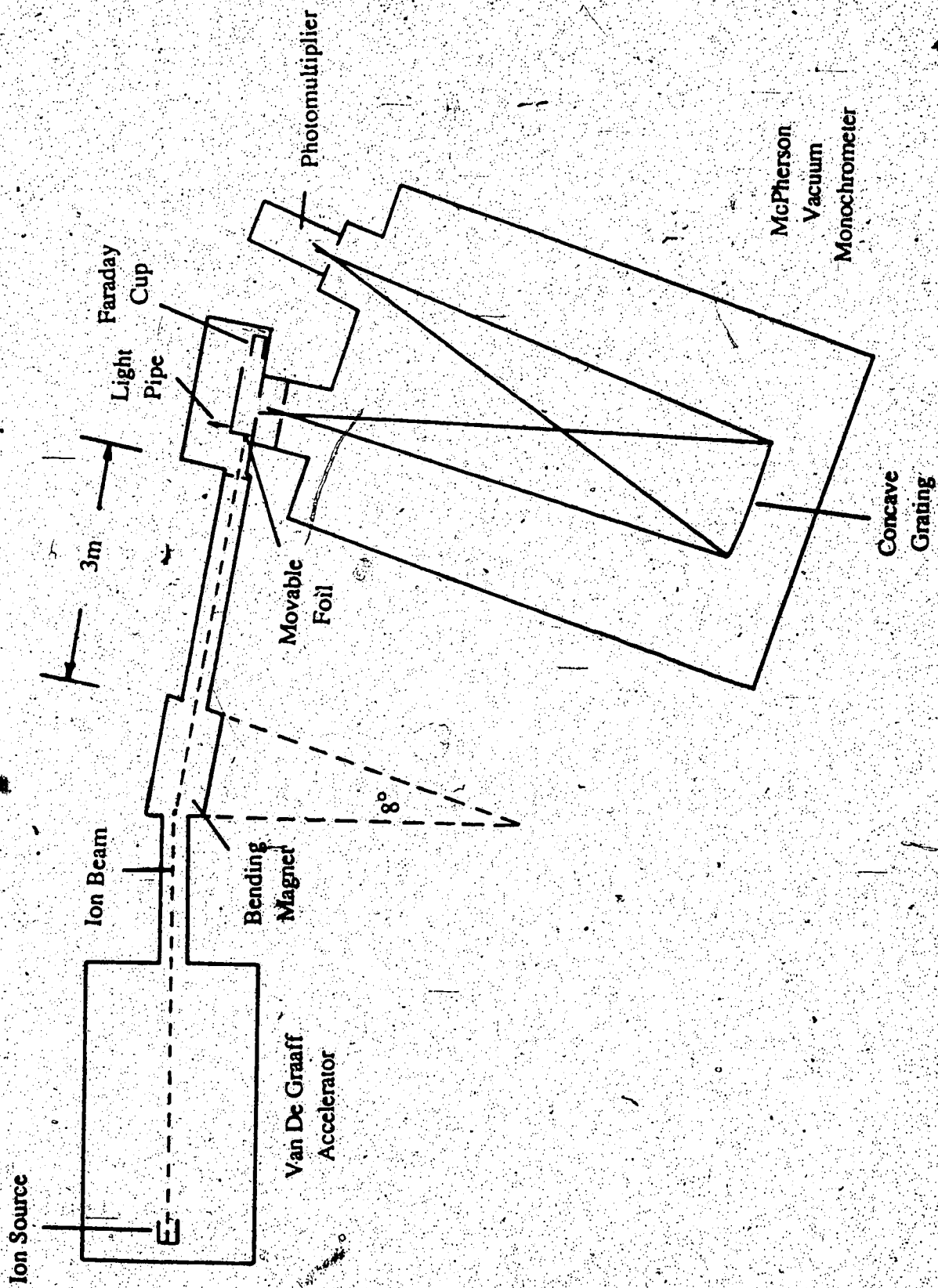
the bombardment, an effective thickness of $10 \pm 5 \mu\text{gm}/\text{cm}^2$ was assumed in estimating the energy loss suffered by the ions at the foil (NS70), yielding a value of 2.75 mm/ns ($\pm 3\%$) for the post-foil velocity of the Ar ions.

The radiation emitted by the foil-excited ions was dispersed by a 1m model 225 McPherson normal incidence spectrometer equipped with gratings blazed at 450A, 1200A and 3000A. Three detectors were used in this experiment, these being a Channeltron electron multiplier for wavelengths below 1050A, an EMR 542G photomultiplier for wavelengths in the range from 1050A to 1650A and an EMI 9789 QB photomultiplier for wavelengths above 1650A.

Two stepping motors, one driving the foil holder and the other the spectrometer grating, were controlled by a TN-11 data acquisition system (PGOK79), which is linked with the university main-frame AMDAHL computer. The position of the foil (or the grating) was recorded simultaneously with the number of photon counts detected per channel. Scanning the foil position or the grating orientation then gave an intensity decay curve or a section of spectrum. The signal was normalized by a second optical detection system, which employed a light pipe (attached to the foil holder) to view the ion beam right after the foil.

FIGURE 2.1

Sketch Of The Data Acquisition System
(not drawn to scale)



2.2 Spectrum Recording

Spectrum recording was performed by fixing the foil position to give the maximum signal intensity and rotating the grating in discrete steps. Spectra were recorded over the wavelength range from 350A to 2450A at the ion energy of 1.6 eV, typically using steps of 0.5A and an instrumental linewidth of 1.0A. (sections of the survey spectra are shown in Appendix I. In BFS, instrumental linewidth is a consequence of two factors. The first factor contributing to the linewidth is the width of the spectrometer slits, which causes a linewidth of $D \times S$, where D is the inverse linear dispersion and S the width of the slits. The second factor is the Doppler broadening caused by the high particle speed and non-zero acceptance angle. In this work the first factor is dominant. It has been shown (SL71) that Doppler broadening can be virtually eliminated by refocusing the spectrometer. In the present experiment, Doppler broadening gave a linewidth that corresponded to a slitwidth much less than the slitwidth actually used (100 μ m) for most of the spectrum (below 1300A), and hence no attempt was made to refocus the spectrometer. (One problem with the refocusing technique is that it must be repeated for each wavelength as the refocusing distance varies linearly with wavelength.)

Additional spectra were recorded at higher resolution for regions of particular interest. Typically, slits of 30 μ m and grating masks of 30mm were used to decrease the

linewidth to 0.35\AA (Doppler broadening corresponded to a slitwidth of around $20\mu\text{m}$ for these measurements.) Two lines around 0.2\AA apart can be well resolved in the high resolution spectra with this system using narrower slits and the second order of diffraction. For second order spectra, the step size of the spectrum was decreased to 0.05\AA . Spectra were also recorded with the foil position 2mm downstream in an attempt to distinguish short-lived from long-lived lines. BFS spectra were recorded at 2.5MeV by Dr. J.P. Buchet (private communication), and at 4.0MeV by Dr. A.E. Livingston (private communication). These spectra proved very useful for CHARGE STATE IDENTIFICATION IN THIS WORK (SEE SECTION 3.2).

2.3 Intensity Decay Curve Recording

Intensity decay curves were recorded by fixing the angle of the grating to view the line of interest and moving the foil holder in discrete steps. In a typical measurement the foil was moved so that observations were made from 0.2mm position upstream of the foil to 5.4mm downstream. This corresponds to an elapsed time of $\sim 2\text{ns}$, i.e. more than 10 mean lives for short-lived lines. For some transitions from long-lived energy levels, decay curves were recorded for about 8ns , which is at least three times the mean life of the energy level involved.

Several step sizes were used in a single decay curve, from the smallest step size of 0.05mm to the largest of 0.4mm. A typical decay curve might consist of 25 steps of 0.05mm, 10 of 0.10mm, 10 of 0.2mm and 5 of 0.4mm. The early section of the decay curve is particularly important for two reasons. Firstly, the lifetimes of most of the lines considered in this program are very short (~ 0.1 ns) and thus most of the important information about such lifetimes lies in the early section of the curve. Secondly, recording the curve in short steps starting upstream of the foil permits the accurate location of the foil position. This is important when decay curves for different transitions are to be analyzed simultaneously, as in an ANDC analysis.

The typical sizes of slit and mask were 200 μ m and 10mm respectively, yielding an effective viewing length of 0.4mm (Fig. 2.2a) following the equation

$$(2.1) \quad \Delta = S + M \cdot R$$

where Δ is the viewing length, S is the slitwidth, M is the width of the grating mask and R is the ratio of two distances from the slit, as shown in Fig. 2.2a. Actually, the detector system views different sections of the ion-beam through the spectrometer with different efficiency, depending on the instrumental "window function" (Fig 2.2b). The recorded signal is determined by the convolution of the multi-exponential decay function and this window function

(TWHB76). Traditionally, multi-exponential curve fitting is only applied to that part of the decay curve that does not include observation of the foil, i.e. points closer to the foil than one-half the viewing length, Δ , are removed prior to fitting. However, the region immediately following the foil is physically very important, especially for short-lived levels. Therefore the window function has been incorporated into the fitting program to include points closer to the foil than one-half the viewing length. Further discussion of this procedure is given in Chapter 4.

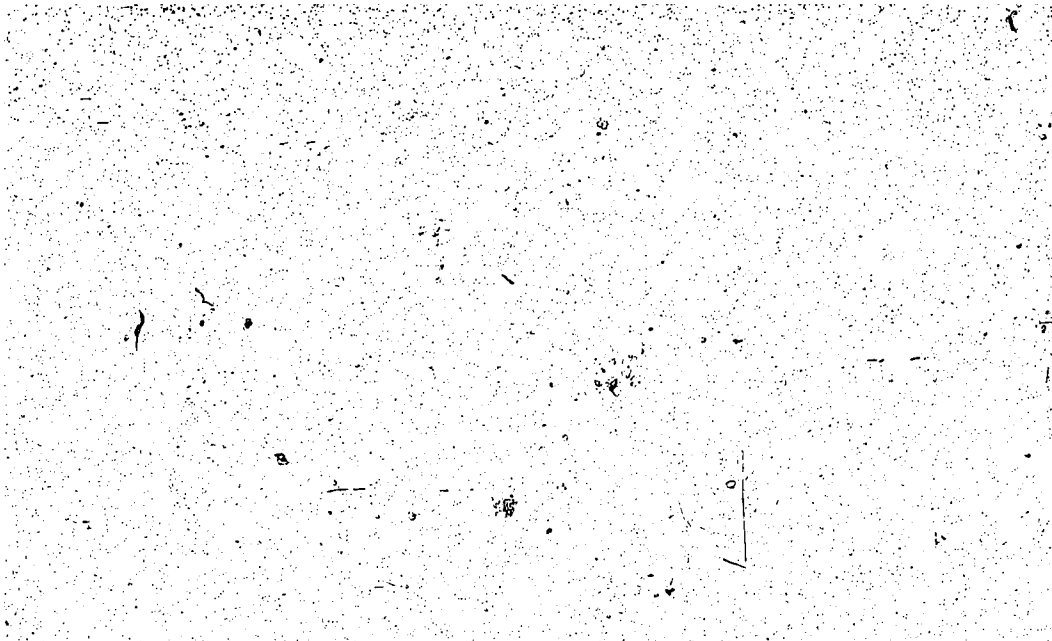
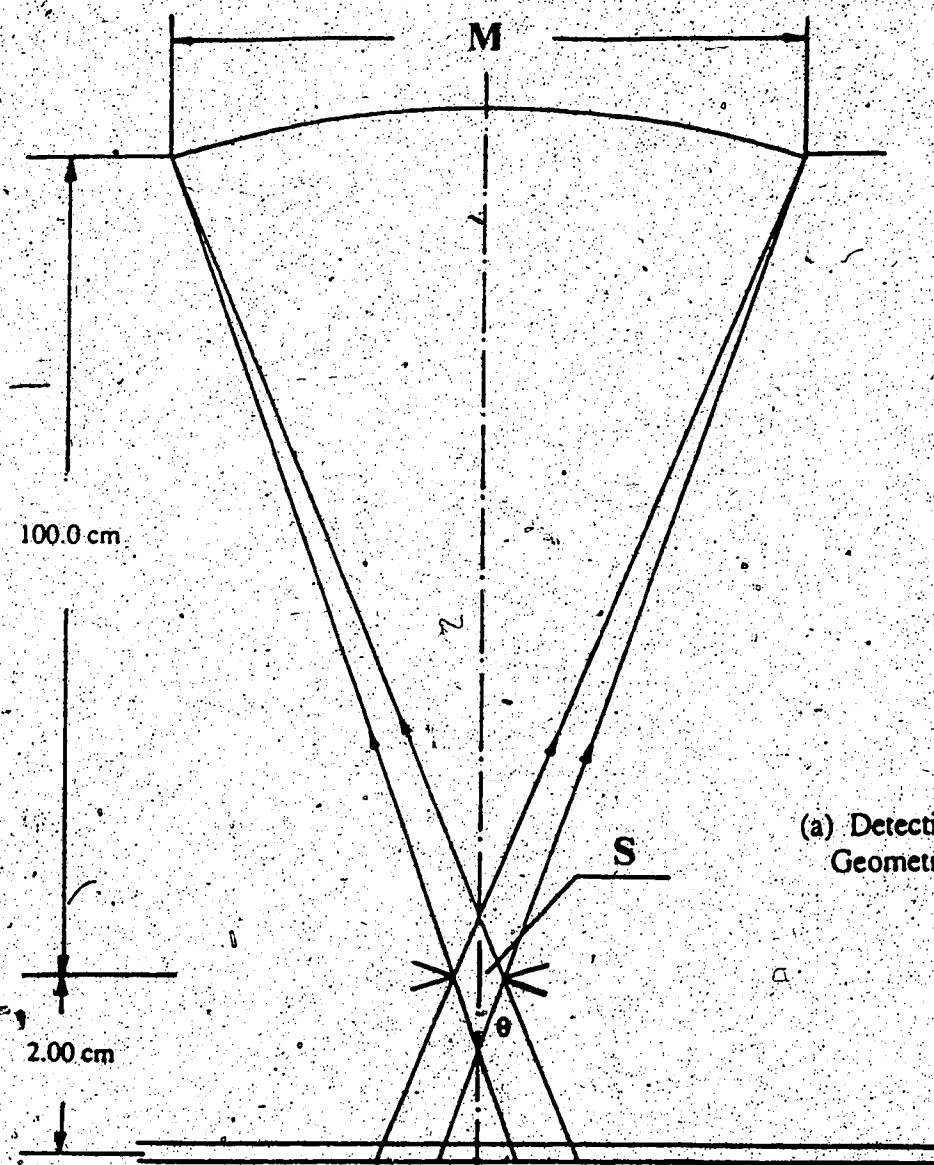


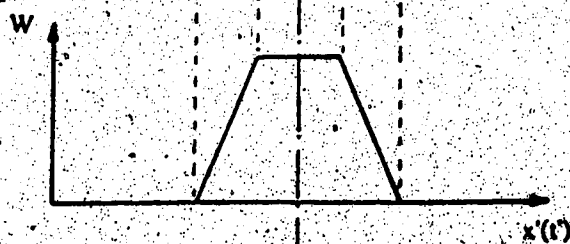
FIGURE 2.2

Detection System Geometry (not drawn to scale)

Showing the contributions to the instrumental window function due to the finite slit width and the finite width of masked grating.



(a) Detection System
Geometry (not to scale)



(b) Window Function

3. SPECTROSCOPIC ANALYSIS

As was mentioned in Chapter 1, many of the energy levels of the $3p^2$ and $3s3p3d$ configurations had not been classified when this project was begun. M.C. Buchet-Poulizac and her colleagues had reported some observed transitions from $3s3p3d$ to $3s3p^2$ levels (BBC82), but their results seemed in marked disagreement with the theoretical calculations. The first step towards the goal of testing the effectiveness of the ANDC technique in determining the lifetimes of $3s3p^2$ and $3s^23d$ levels in ArVI was therefore to locate the cascade transitions from the $3p^2$ and $3s3p3d$ levels. The methods used to locate these energy levels will now be discussed. Firstly, an initial estimate of the level energies was obtained by using the sequence trend method. A computer program was then used to search for possible energy levels together with the important transitions decaying into the resonance levels. Finally, some spectra with higher resolution were taken to confirm the possible assignments.

3.1 All Isoelectronic Sequence Trends

The All sequence consists of ions having three active electrons. Despite the interaction between different configurations within the $(n=3)$ complex, the results of the theoretical calculation, which included the configuration-interactions within this complex, give smooth

sequence trends (Fig. 3.1-3.2). On the experimental side, most of these levels belonging to the $3p^3$ and $3s3p(^3P)3d$ configurations have been assigned for the lower Z members of the All sequence up to ClV (Mo49, Ke68, BM71, BDG82, MZ77, BBL73). In addition, Pinnington et al have recently reported all the doublet energy levels of the $3p^3$ and $3s3p3d$ configurations for TiX (PATH87). An initial estimate for the energy of a given level in ArVI was obtained by comparing the theoretical and experimental data for that level along the All isoelectronic sequence, as shown in Figs. 3.1 and 3.2.

It is striking that the experimental results give rather irregular trends if all the previous assignments are accepted (Figs. 3.1, 3.2). In some cases, the agreement with the theoretical calculations is quite good while in other cases the agreement is rather poor. The calculations show that the $3p^3$ and $3s3p(^3P)3d$ configurations are so strongly mixed that labelling of the 3P and 3D levels belonging to these configurations for low Z members is a matter of taste. However, for medium and high stages of ionization, the assignments are unambiguous as the leading term in each of the mixed states is quite dominant. In the present work, the assignment suggested by the theoretical analysis is given to the experimentally determined energy levels in Figs. 3.1 - 3.2. In particular, the assignments of the lowest four levels assigned in this work are labelled $3p^3$, whereas Buchet-Poulizac et al. (BBC82) had given them

the label 3s3p3d.

3.2 Energy Dependence of Spectral Line Intensity

Beam-foil emission spectra strongly depend on the ion beam energy. The intensity of a specific line obviously depends on the population of the upper energy level involved, which is itself a function of the energy. The method of identifying the charge state for a given spectral line, by comparing the relative intensities with the incident ion energy, was first suggested by Kay (Ka65). Spectra have been recorded previously in this laboratory for Ar⁺ ions of energies ranging from 0.2MeV to 1.8MeV (Li74). The ArI and II lines are dominant at energies below 0.4MeV while ArVI, VII and VIII are dominant at 1.8MeV. It is known (SM86, SW69) that Ar⁵⁺ ions will be most abundant after foil ionization when the incident energy is around 3MeV, the Ar⁵⁺ component then being around 26%. For this present work, 1.64MeV was the highest energy for which a strong and stable ion beam could be obtained from the accelerator (tests with an incident beam of Ar²⁺ ion gave an ion beam that was too weak and unstable). At 1.64MeV, the composition of the post-foil beam will be approximately 3% (Ar⁺), 12% (Ar²⁺), 24% (Ar³⁺), 27% (Ar⁴⁺), 19% (Ar⁵⁺), 10% (Ar⁶⁺) and 3% (Ar⁷⁺). Clearly, lines of charge states other than Ar⁵⁺ also show in the spectra. Therefore charge identification is

FIGURE 3.1

Isoelectronic Sequence Trends for
the $3p^2$ and $3s3p(^3P)3d^2$ 3P , 3D Terms

The dashed curve represents the MCDF calculation of Huang(Hu86) and ■ the CI-calculation of Fawcett using scaled Slater integrals(Fa83). The experimental points are from references given in the text(O), J.P. Buchet(x private communication) and this work(●).

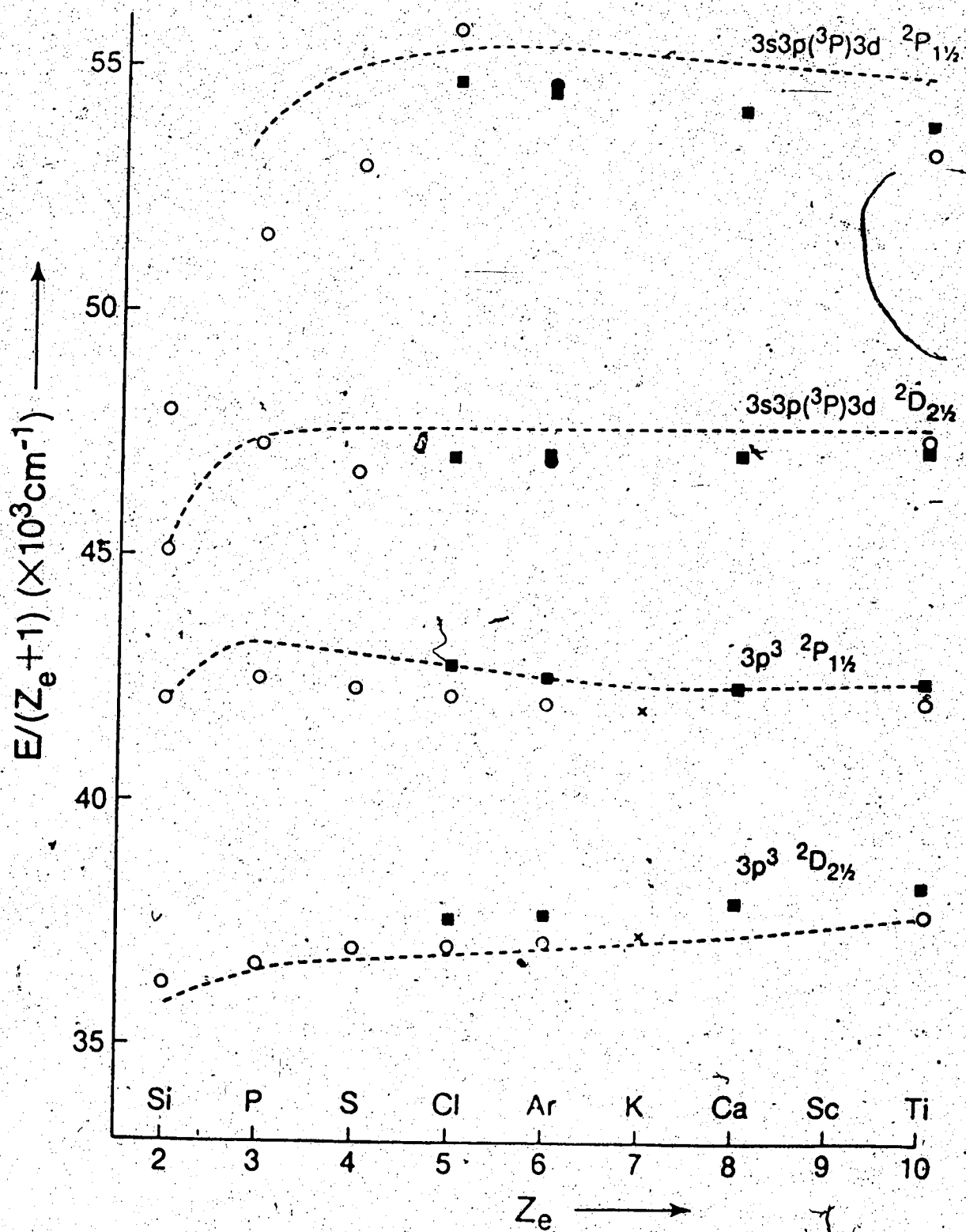
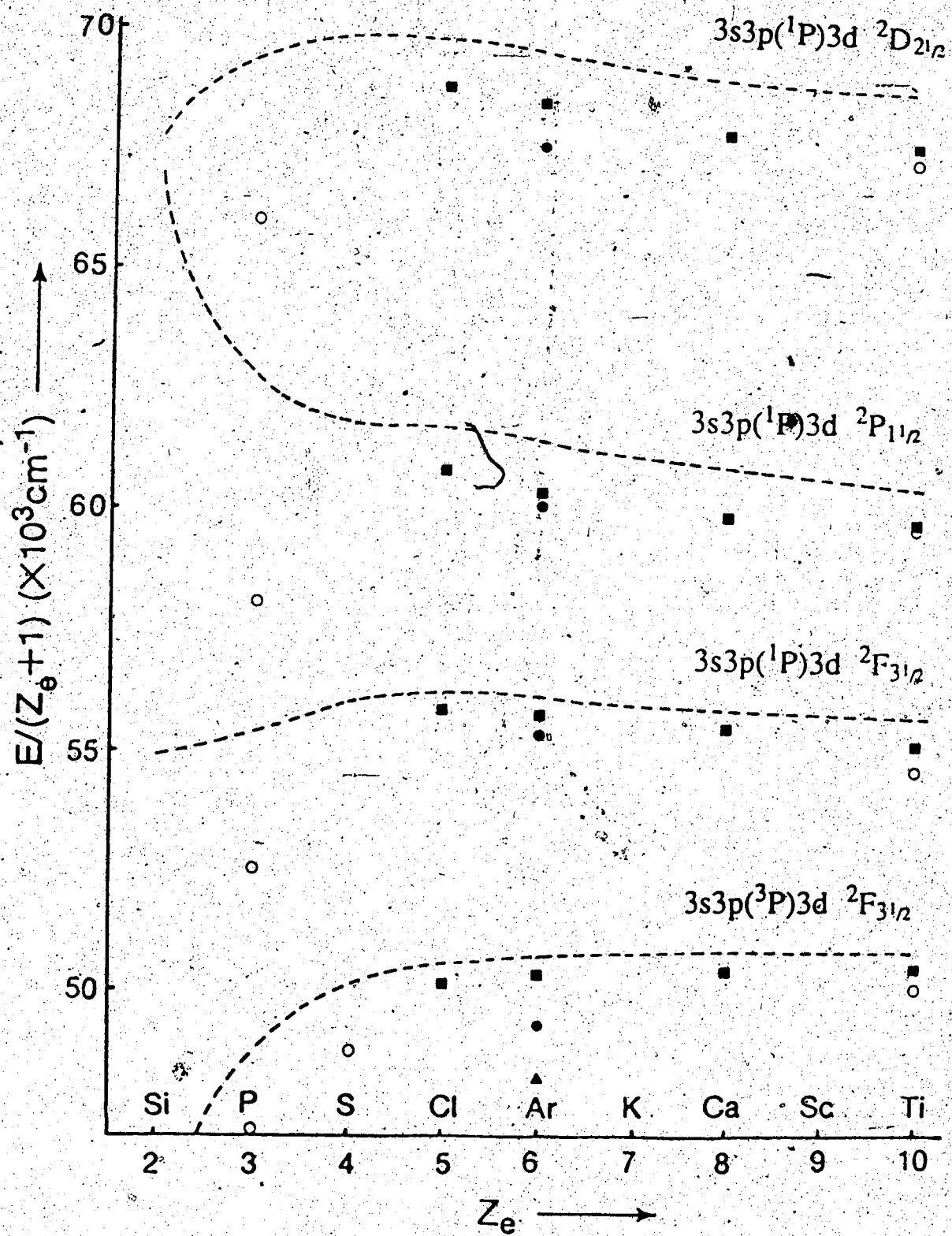


FIGURE 3.2

Isoelectronic Sequence Trends for
the $3s3p(^1P)3d\ ^1F$ and $3s3p(^1P)3d$
Doublet Terms

- * The dashed curve, ■, ○ and ● represent the same as in Fig. 3.1.
- ** The data for $3s3p(^1P)3d\ ^1D$ ($J=5/2$) are shifted upwards by 11000 cm^{-1} , and that for $3s3p(^1P)3d\ ^1P$ ($J=3/2$) are shifted upwards by 3000 cm^{-1} for clarity of presentation.
- {*** ▲ represents the suggested assignment for $3s3p3d\ ^1F$ ($J=7/2$) by Buchet et al. (BBC82).



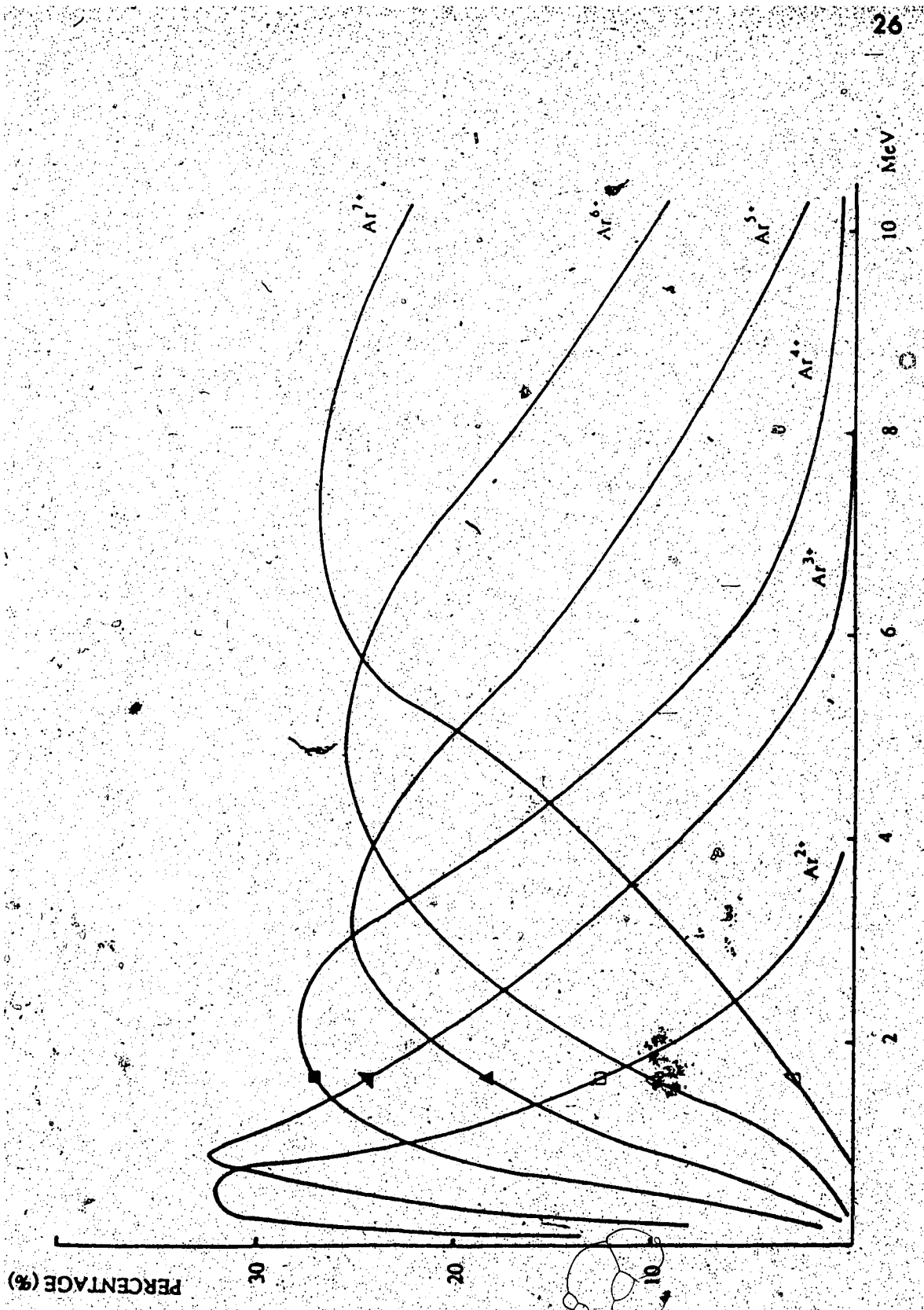
necessary in this work.

From Fig. 3.3, the abundance of Ar^{3+} begins to decrease at around 0.8MeV, while that of Ar^{2+} does so at around 0.5MeV. Since the peak ArVI abundance is located at around 3MeV, a study of the relative intensities of spectral lines at different energies below 2.5MeV will distinguish Ar^{2+} , Ar^{3+} from Ar^{5+} lines. As the ArIII spectrum is very rich, most of the individual ArIII lines are relatively weak in the spectra at 1.64MeV. On the other hand, because of their simpler electronic structures, the spectra for ArVII and VIII give relatively few but intense lines at 1.64MeV. Distinguishing Ar^{6+} from Ar^{5+} is helped by comparing relative intensities in spectra at 1.64MeV, 2.5MeV, and 4.0MeV, since the abundance of ArVI begins to decrease at around 3.0MeV while that of ArVII is increasing during the whole range between 1.64 and 4.0MeV (Fig. 3.3). For example, identification of the charge state responsible for 509A was not clear before this work. Livingston (Li74) had suggested that ArVII was responsible, while Lévêque et al. (LGR84) had suggested ArVI. The ratio of intensities of the lines found at 509.0A and 501.1A, which is identified as an ArVII line (Li74, LGR84, BBC82), does not change significantly in spectra at low energy, but it is a function of energy at higher energy, being around 1:1, 1:2, and 2:5 at 1.64MeV, 2.5MeV and 4.0MeV respectively.

The major problems occurred in the identification of weak lines, especially when these lines were located close

FIGURE 3.3

Energy Dependence of the Ar
Charge State Distribution after the Foil



to a strong line the wings of which may contribute some background to the weak line. For example, the line at 502.3A had been suggested as an ArV line (LGR84). This line is close to the strong ArVII line at 501.0A line. The intensity ratios between the 502.3 and 509.0A are approximately 1:4, 2:9 and 2:7 at 1.64MeV, 2.5MeV and 4.0MeV respectively. This line therefore seems more likely to be an ArVI line.

However, this analysis was not conclusive because of the weakness of the line at 502.3A and the perturbing effect of the nearby strong ArVII line. Further evidence that this line does belong to ArVI is given below (see Section 3.5).

Charge state analysis for the lines studied in this work are generally in accordance with suggestion made by J.P. Buchet (private communication) and other works (Li74, LSR84, Sc65).

3.3 Computer Spectral Analysis

The $3s3p^2 \ ^2P$ and $3s^23d \ ^2D$ levels were classified by Phillips et al. (PP41) and Fawcett et al. (FJW61). Fawcett's calculation (Fa82) includes gf-values for all the important transitions between the $3p^2$, $3s3p3d$ and resonance levels, and yields estimates of the intensity of these transitions and the lifetimes of the levels of the upper levels (Table A4.1). If a given level makes two or more important transitions into known energy levels, transitions are expected to appear in the spectrum having energy differences

corresponding to the separation of the known levels. A computer program using this principle (Level:Search, see Appendix II) was written to search for the required energy levels of the $3p^2$ and $3s3p3d$ configurations, using Fawcett's calculation of which transitions should appear in the spectra.

The main idea of this program is to scan the lines in the wavelength regions estimated by Fawcett or by the sequence method (Section 3.1). One of these seven resonance levels is used as a reference level. In scanning, if lines are found having energy differences corresponding to the differences between the reference level and other resonance levels, the energy of the new upper level suggested by the analysis together with the wavelengths of the transitions from it will be listed. In this way, the $3p^2$ 3P and 1D levels were found immediately, together with 12 transitions from them to the resonance levels (Table 3.1).

3.4 Level Confirmation by Decay Curve Comparison

Transitions from the same upper level into different levels should not only show the same lifetime from the m-e analysis but also the same shape for their intensity decay curves. This can be used to provide further evidence for the new assignments suggested from the spectroscopic techniques discussed in the previous section.

As was mentioned in Chapter 1, multi-exponential fitting techniques must be used to analyze the intensity decay curve for these lines. Such analyses often yield results with relatively large uncertainties, particularly for weak lines. Furthermore, lines of similar wavelength often show similar lifetimes, so that simple comparison of the lifetimes obtained by m-e fitting may not be very conclusive in deciding possible assignments. Comparison of the decay curves themselves can be a much more sensitive test, since it includes the effects of cascading over the whole curves. On the other hand, if line blending is present, decay curve comparison may be less conclusive than normal m-e fitting techniques. In general, both primary lifetimes and decay curve shapes should be compared in testing whether a given pair of transitions do come from a common upper level.

A computer program (TFIT) was developed here in 1986 to permit decay curve comparison. The principle of this program is similar to the multi-exponential fitting program, TROY, except that the TROY fitting parameters for one possible branch transition from the postulated upper level are used as fixed parameters to fit the other branches, with only the absolute intensity and beam velocity as free parameters. In other words, the scales of the intensity and time axes are allowed to vary, but the fundamental shape of the decay curve is fixed. If the decay curve being tested is from the same upper level as the first curve (represented by the

HOMER/TROY parameters), the ratio of the fitting and actual beam velocities should be close to unity. However, line blending, the statistical nature of the data and the experimental conditions (such as foil thickness, the instrumental viewing length, the precise setting of the spectrometer etc.) can effect the TFIT results. As a test, this program was employed to compare the known intense branches from the $3s3p^2$ 2S , 2P , 2D and $3s^23d$ 2D resonance lines. The velocity ratios fell in the range of 0.8 to 1.2 in this test. Large discrepancies were found when blending was present. It was therefore decided to accept TFIT analyses only when the ratio was found to lie in the range of 0.8 to 1.2. Detailed discussions are shown in Appendix III. In general, this method can provide corroboration for new assignments, but it is not always conclusive, particularly when one of the lines being compared is very weak. Analysis giving strong support to the assignments for the $3p^2$ 2P , 2D , $3s3p(^2P)3d$ 2P and 2F levels will be discussed in the next section.

3.5 Assignment for the $3p^2$ and $3s3p3d$ levels

3.5.1 $3p^2$ Levels

The assignment of the $3p^2$ levels was found to be relatively straightforward. The transitions from these levels are relatively strong and generally fall in uncrowded

regions of the spectrum, so that the levels were easily located using the procedure described in Section 3.3. Two spectral regions (around 619A and 783A) were recorded at higher resolution. The first of these spectra shows that the single wide line at 619.0A found in the survey spectra actually consisted of two lines at 618.65 (peak A) and 619.20A (peak B), with a ratio of intensity around 3:5 (Fig. 3.4). This is in good agreement with Fawcett's calculation (Table A4.1), thus supporting the assignments to the transitions from $3p^3 \ ^3P$ ($J=1/2$) to $3s3p^2 \ ^3D$ ($J=3/2$) and from $3p^3 \ ^3P$ ($J=3/2$) to $3s3p^2 \ ^3D$ ($J=5/2$) respectively. The second of these higher resolution spectra (Fig. 3.5) for the region around 783A again shows fine structure splitting, 783.1 (peak A) and 783.7A (peak B). The relative intensities of these lines are in agreement with the predictions of Fawcett.

Decay curve comparison (TFIT) was also applied for the transitions from the $3p^3 \ ^3P$ levels (at 905 and 619A) and the transitions from the $3p^3 \ ^3D$ levels (at 783.5, 1284 and 1304A). The results yielded strong support for the assignments (Appendix III).

3.5.2 $3s3p(^3P)3d$ Levels

Most of the important transitions from the $3s3p(^3P)3d$ levels are unfortunately located in rather crowded spectral regions. It is, of course, more difficult to use the scanning computer program if the lines are not well

resolved. In the case of the $3s3p(^3P)3d\ ^3D$ levels, only one transition from each level is important, and the wavelengths of these transitions are so close that only one decay curve was recorded from this doublet. Hence the TFIT program is not applicable, and the scanning program is less definitive. Spectra with higher resolution were necessary to identify the closely-spaced doublet expected for the multiplet $3s3p\ ^3D - 3s3p(^3P)3d\ ^3D$. In the second order spectrum around 509.0Å, a single wide line in the survey spectra was resolved into two lines, 508.9 (peak A) and 509.2Å (peak B), with a separation of around 0.30Å (Fig.3.6). The intensity ratio of these two lines is approximately 5:7 which is in good agreement with Fawcett's calculation (Table A4.1). A weak transition was then found at 687.90Å, which is the wavelength corresponding to the transition from $3s3p(^3P)3d\ ^3D$ ($J=5/2$) to $3s3p\ ^3P$ ($J=3/2$).

Buchet et al. had suggested an assignment for the $3s3p3d\ ^3F$ ($J=7/2$) level (BBC82), but this gives poor agreement with the sequence trend (Fig. 3.1). A decay curve was recorded at 486.7Å, the transition assigned by Buchet et al. from $3s3p3d\ ^3F$ ($J=7/2$) to $3s3p\ ^3D$ ($J=5/2$), yielding an approximate lifetime of 0.05ns, which is quite different from the theoretical prediction (0.125ns). Furthermore, no transitions could be found corresponding to the branch down to $3s^23d\ ^3D$ ($J=5/2$) or to the transitions from 3F ($J=5/2$) to either $3s3p\ ^3D$ ($J=3/2$) or $3s^23d\ ^3D$ ($J=3/2$), assuming that the 3F splitting is close to the theoretical calculation by

Fawcett (Fa83). The suggested assignment by Buchet et al. therefore appears to be incorrect.

In the search for the $3s3p(^1P)3d\ ^2P$ and 2F levels, a spectrum was recorded in increments of 0.2A from 468 to 480A (Fig. 3.7). Two lines (peaks A and B) in this region were assigned to transitions from the 2P levels, and two lines (peaks C and D) to transitions from the 2F levels (Table 3.1). Intensity curves were recorded for four of the transitions expected from the postulated 2P levels (at 468.5, 469.85, 497.4, and 502.3A). TFIT analysis gave satisfactory results for these decays (see Appendix III). The lines found at 470.9 and 792.0A were assigned as the transitions from $3s3p(^1P)3d\ ^2F$ ($J=7/2$) to $3s^23d\ ^2D$ ($J=5/2$) and $3s3p^2\ ^2D$ ($J=5/2$), while the line of 476.8A was assigned as the transition from the 2F ($J=5/2$) to the $3s3p^2\ ^2D$ ($J=3/2$) levels. Intensity decay curves were recorded for these three lines. TFIT analyses also support these assignments (Appendix III). However, it should be mentioned that the transition from this newly assigned $3s3p(^1P)3d\ ^2F$ ($J=5/2$) level to $3s^23d\ ^2D$ ($J=3/2$) (at 809.1A) is found to be weaker than calculation (Fa82) predicts.

3.5.3 $3s3p(^1P)3d$ Levels

Similar procedures have been followed in search of the $3s3p(^1P)3d$ levels, although the results of these analyses are less conclusive than for the $3s3p(^1P)3d$ levels just discussed. A second order spectrum was recorded around

594.10A, a known intense line of ArVI. A line at 594.8A, which had been blended in the survey spectra, was resolved. This line and another line at 592.9A were assigned as the transitions from $3s3p(^1P)3d^2F$ to $3s^23d^2D$, based on Fawcett's calculation. From the assigned $3s3p(^1P)3d^2F$ levels, other transitions could also be assigned in the spectrum at 392.5 and 393.6A (see Table 3.1). Decay curves were recorded for the lines at 594.8, 592.5 and 393.6A, and the shapes of decay curves were compared by the TFIT program. The results show that decay curve of 592.5 is similar to that of 594.8A (Appendix III), but quite different from that of 393.6A. This is possibly caused by blending at 393.6A and/or at 592.5 and 594.8A. Furthermore, the 592.5A line seems too strong compared with 594.8A, so it is certainly possible that it is blended with an unknown line. These identifications are thus very tentative.

For the $3s3p(^1P)3d^2D$ term, the strongest line should be the transition from $3s3p(^1P)3d^2P$ ($J=5/2$) down to the $3s3p^2^2P$ ($J=3/2$). A line at 472.1A was found that could be this transition. Two lines at 574.0 and 477.7A have been assigned as the transitions from the $3s3p(^1P)3d^2D$ ($J=3/2$) down to the $3s^23d^2D$ ($J=5/2$) and $3s3p^2^2P$ ($J=3/2$) levels respectively. The intensity ratio of lines at 477.7 and 472.1A is approximately 1:4, which is in fair agreement with Fawcett's calculation (Table A4.1). However, the transitions then expected at 574.0 and 565.6A from these levels down to

FIGURE 3.4 - 3.5

Spectra

In Figure 3.4 (second order diffraction), the H I line at 1215.67Å (not shown in figure) is used as a calibration line.

In Figure 3.5 (second order diffraction), the Ar VIII line at 526.46Å (C, third order diffraction) is used as a calibration line.

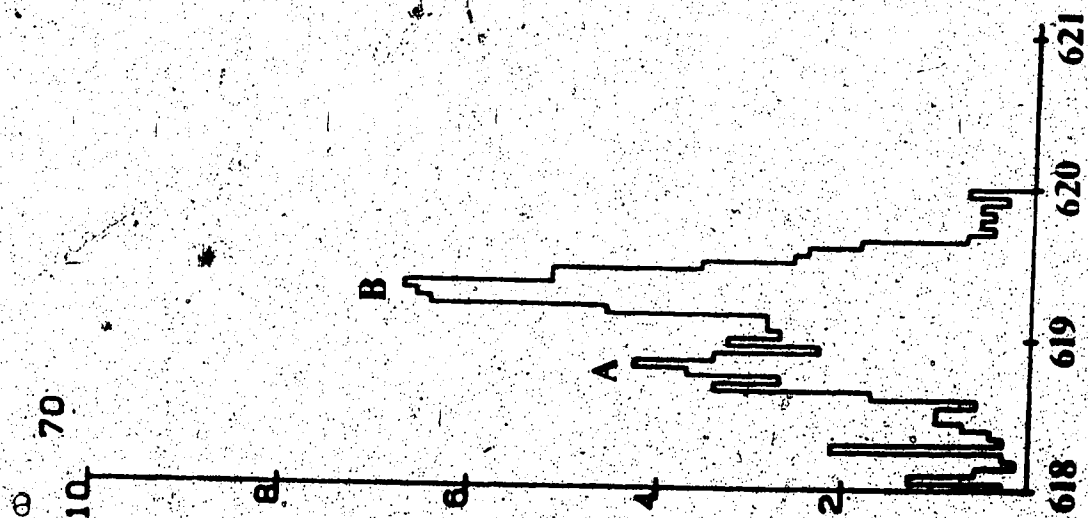


Fig. 3.4

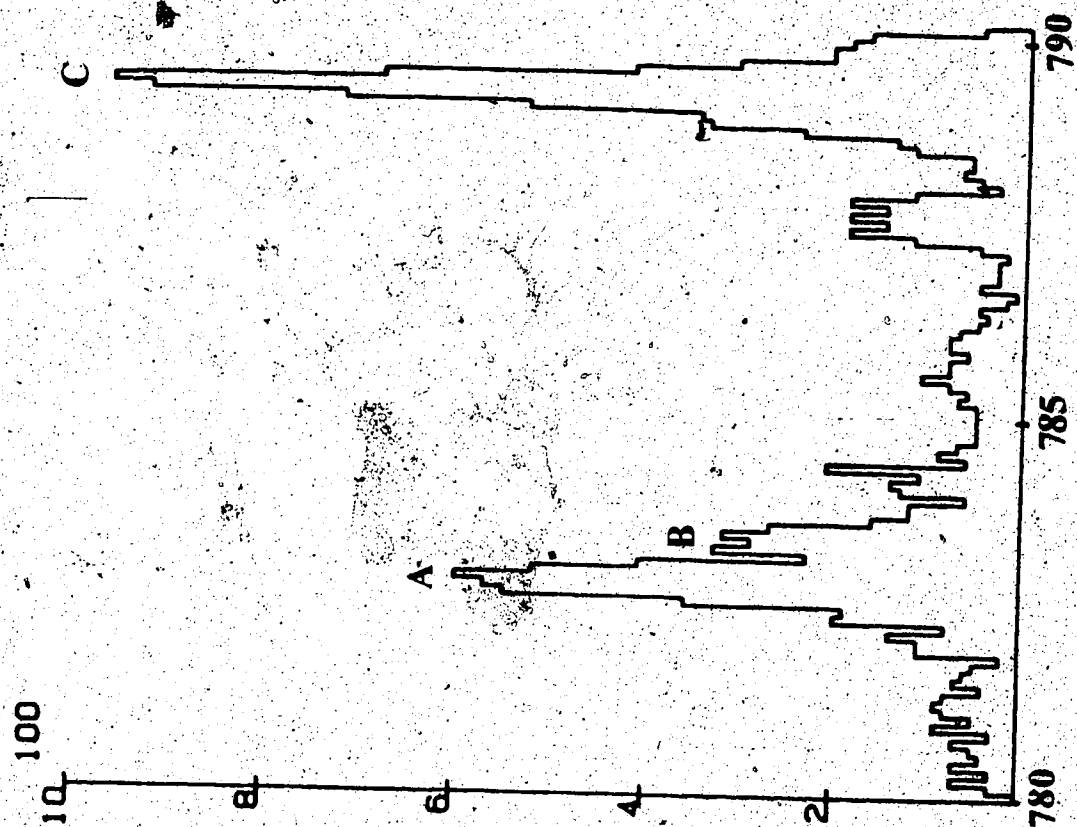


Fig. 3.5

FIGURE 3.6 - 3.7

Spectra

In Figure 3.6 (second order diffraction), the ArVIII line at 519.43A (not shown in figure) is used as a calibration line.

In Figure 3.7, the ArVIII line at 479.38A (E) is used as a calibration line.

SQUARE ROOT PLOT

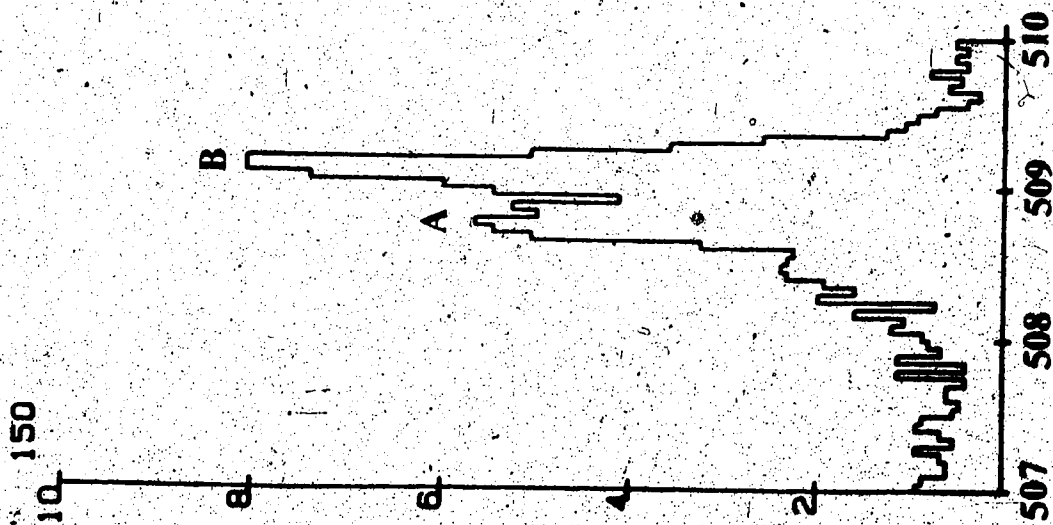


Fig. 3.6

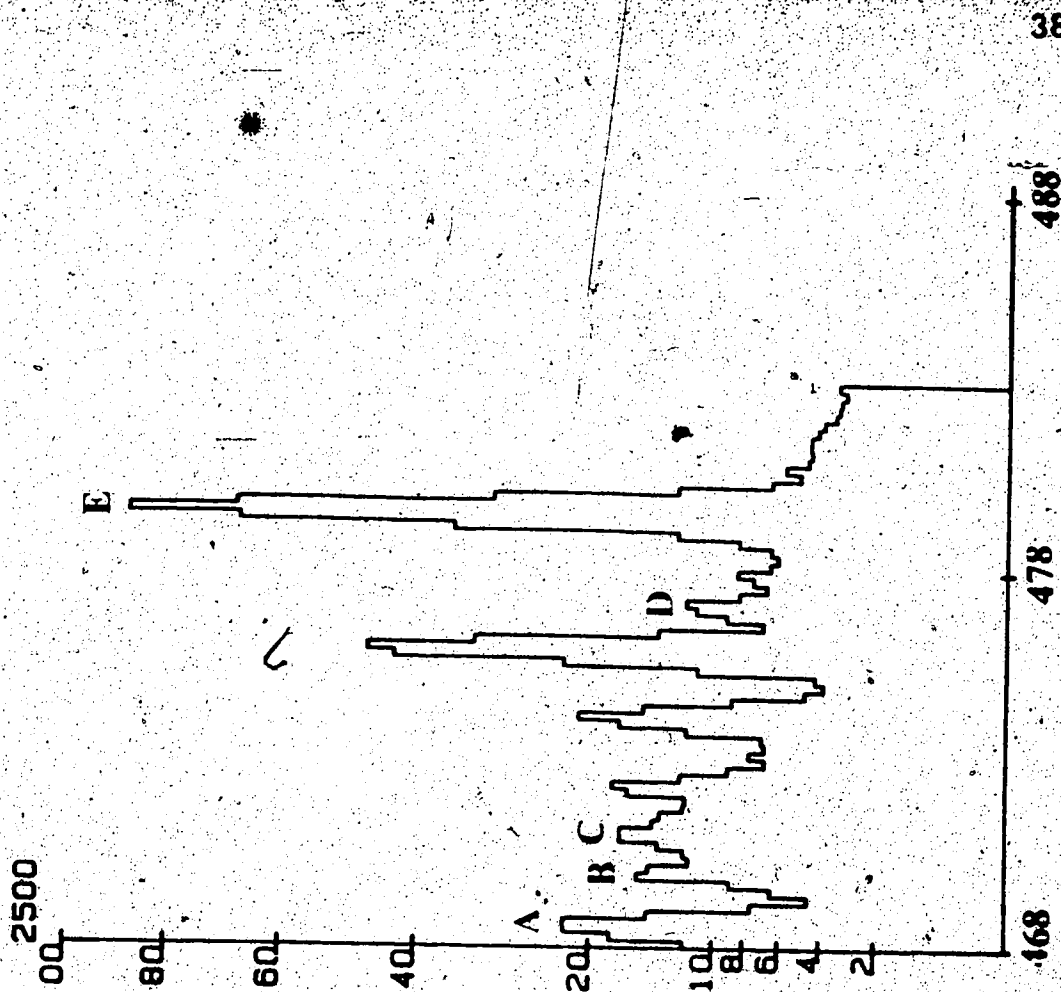


Fig. 3.7

$3s^2 3d\ ^2D$ ($J=5/2$), appear weaker than theoretical predictions. An intensity decay curve was recorded for the relatively intense line at 472.1A only, and hence no TFIT test could be made in this case.

It appears that there may also be a problem in locating the $3s3p(^1P)3d\ ^3P$ levels. From the theoretical prediction, the strongest transition from these levels is that from $3s3p(^1P)3d\ ^3P$ ($J=3/2$) down to $3s3p^2\ ^3P$ ($J=1/2$). However, no such line could be found in the expected region that gave the expected corresponding branch transitions. On the other hand, the following argument suggests that it is possible that this transition is blended with the strong ArVI line at 459.32A. The next two strongest transitions should be from the 3P levels down to the $3s^2 3d\ ^2D$ ($J=3/2$). A line at 557.1A was tentatively assigned as the transition from 3P ($J=1/2$) down to $3s^2 3d\ ^2D$ ($J=3/2$). Two other weak transitions from this assigned level to the $3s3p^2$ levels could be found in the spectra at 463.2 and 466.2A. Using the energy suggested by the 557.1A line for the 3P ($J=1/2$) level and Fawcett's estimate of the 3P fine-structure splitting, it is expected that the ($J=3/2$) level lies at $400600 \pm 2000 \text{ cm}^{-1}$. If this is the case, the three strongest transitions from this level would all be masked by strong, classified ArVI lines at 459.32, 462.01 and 551.37A. The intensity decay curve could be recorded only for the line at 557.1A from this doublet, so that again no TFIT analysis was possible.

3.5.4 Summary of the Spectroscopic Assignments

In this work, spectroscopic assignments for 30 transitions of ArVI were suggested, with 15 levels of the $3p^1$ and $3s3p3d$ electron configurations being derived from these transitions. When two or more transitions from the same level were assigned, the method of least squares was used to deduce the energy of this level. The results are shown in Table 3.2. It is interesting to note that the weighted mean of the ratio of the observed and the calculated energy levels (Fa83) is 0.988 ± 0.006 , while the weighted mean of the corresponding ratios for the doublet splitting is 1.05 ± 0.25 . The theoretical predictions (Fa83) for the isoelectronic ions TiX, show a similar degree of accuracy (PAHH87). Furthermore, all the inverted doublet terms were correctly predicted by Fawcett (Fa83), as was in the case of TiX. Further support for these assignments is provided by the lifetime analyses which are to be discussed in Chapter 5. The results of all the various approaches described in this chapter support the assignments of the $3p^1$ 1P , 1D and $3s3p(^1P)3d$ 1P , 1D , 1F levels. The assignments for these levels thus appear acceptable. The situation is much less definite for the other six levels considered. Because of the weakness of most of the transitions from the $3s3p(^1P)3d$ 1P and 1D levels, intensity decay curves were only measured for one relatively strong transition from each doublet. Furthermore, some transitions from these assigned levels appeared to be weaker than would be expected from the

theoretical predictions. Further spectroscopic information is clearly required before these assignments can be accepted. The $3s3p(^1P)3d\ ^2F$ levels were also only assigned tentatively, as there are inconsistencies, both in TFIT results and the intensity ratio for the 2F assignments.

Table 3.1

Suggested Assignments for Some ArVI Transitions

Transition			Wavelength (Å)*
3s3p ²	² D 3/2 - 3s3p(¹ P)3d	² F 5/2	392.50 ± 0.30
	² D 5/2 -	² F 7/2	393.55 ± 0.25
	² S 1/2 - 3s3p(³ P)3d	² P 1/2	468.50 ± 0.20
	² S 1/2 -	² P 3/2	469.85 ± 0.20
	² D 5/2 -	² F 7/2	470.90 ± 0.30
	² P 3/2 - 3s3p(¹ P)3d	² D 5/2	472.10 ± 0.20
	² D 3/2 - 3s3p(³ P)3d	² F 5/2	476.80 ± 0.30
	² P 3/2 - 3s3p(¹ P)3d	² D 3/2	477.70 ± 0.30
	² P 1/2 - 3s3p(³ P)3d	² P 1/2	497.40 ± 0.30
	² P 3/2 -	² P 3/2	502.30 ± 0.20
	² D 3/2 -	² D 3/2	508.93 ± 0.15
	² D 5/2 -	² D 5/2	509.25 ± 0.15
3s ² 3d	² D 3/2 - 3s3p(¹ P)3d	² P 5/2	557.10 ± 0.20
	² D 5/2 -	² D 3/2	574.00 ± 0.40
	² D 3/2 -	² F 5/2	592.90 ± 0.20
	² D 5/2 -	² F 7/2	594.80 ± 0.20
3s3p ²	² D 3/2 - 3p ³	² P 1/2	618.65 ± 0.15
	² D 5/2 -	² P 3/2	619.20 ± 0.15
	² P 3/2 - 3s3p(³ P)3d	² D 5/2	687.90 ± 0.30
	² D 3/2 - 3p ³	² D 5/2	782.40 ± 0.20
	² D 5/2 -	² D 5/2	783.10 ± 0.30
	² D 3/2 -	² D 3/2	783.70 ± 0.20
	² D 5/2 -	² D 3/2	784.40 ± 0.20

Table 3.1(Contiune)

Transition			Wavelength (A)*
3s ² 3d	² D 5/2 - 3s3p(² P)3d	² F 7/2	792.00 ± 0.30
3s3p ²	² S, 1/2 - 3p ²	² P 1/2,3/2	804.50 ± 0.30
	² P 1/2 -	² P 1/2,3/2	893.70 ± 0.30
	² P 3/2 -	² P 1/2,3/2	905.00 ± 0.30
	² P 1/2 -	² D 3/2	1283.95 ± 0.15
	² P 3/2 -	² D 5/2	1303.90 ± 0.15
	² P 3/2 -	² D 3/2	1307.50 ± 0.30

* Least-squares fitting of these observed wavelength to the energy-level scheme shown in Fig. A4.1 gives the energy levels listed in Table 3.2. Using these energy levels to calculate the wavelengths gives values which in all cases agree with those shown here well within the quoted uncertainties.

Table 3.2
Suggested Energy Level Assignments for ArVI

Term	J	Energy (cm ⁻¹)	
		This Work	Theory ^a
3p ³	² D 3/2	260065 ± 15	263818
	5/2	260270 ± 20	264049
3p ³	² P 1/2	294095 ± 20	298119
	3/2	294080 ± 20	298078
3s3p(¹ P)3d	² P 1/2	383240 ± 75	382153
	3/2	382650 ± 60	381400
3s3p(³ P)3d	² D 3/2	328955 ± 60	329393
	5/2	328945 ± 60	329376
3s3p(¹ P)3d	² F 5/2	342200 ± 100	350171
	7/2	344915 ± 50	352041
3s3p(¹ P)3d	² P 1/2	398095 ± 65	398919
	3/2	----- b	401467
3s3p(³ P)3d	² D 3/2	392890 ± 100 ^c	399222
	5/2	395400 ± 100 ^c	401843
3s3p(¹ P)3d	² F 5/2	387255 ± 55 ^d	390158
	7/2	386770 ± 55 ^d	389668

a. Configuration-interaction calculation using scaled Slater integrals. (Pa83)

b. All three important transitions expected from this level appear to be masked with the strong classified ArVI lines at 459.3, 462.1 and 551.4Å, in which case its energy must be 399950 ± 200 cm⁻¹ (see text).

c. Several transitions expected from these levels appear anomalously weak in our spectra.

d. Tentative assignments only as TEIT analyses are inconsistent

4. TECHNIQUES FOR DECAY CURVE ANALYSIS

Intensity decay curves were recorded for the resonance transitions from the $3s3p^2$ and $3s^23d$ levels, as well as for the direct in-shell cascades from the levels of the $3p^3$ and $3s3p3d$ configurations. Several techniques were used to analyze these decay curves. These techniques will be briefly reviewed in this chapter.

4.1 Multi-Exponential Curve-Fitting Techniques

Intensity decay curves obtained using beam-foil excitation may best be represented as sums of exponentials because of the non-selective nature of the excitation process. A variety of computer routines has been used to analyze such data sets, examples being HOMER (IL74), TROY (PGOK79) and DISCRETE (Pr76). In this work, HOMER and TROY were normally used to analyze the data, while DISCRETE was used as a check.

A typical curve contains a set of N triads (y_i, x_i, t_i) where y_i is the number of photons recorded by the detector at the downstream position x_i in the time period t_i that is required to accumulate a fixed number of photons in the optical normalization channel. The counting number y_i is assumed to be subject to fluctuations described by the Poisson distribution, while the x_i and t_i are assumed to have negligible error.

Both HOMER and TROY are designed to find the function which best fits the recorded set of N triads.

$$(4.1) \quad f_i = \sum_{j=1}^m A_j \exp(-x_i/v \cdot T_j) + C_i,$$

where m is the number of terms, v is the known ion velocity, T_j is the lifetime of component j , and C_i is the dark count which is proportional to the counting period t_i , and the A_j 's are the amplitudes which depend on the excitation conditions. As in all least-squares fitting techniques, the approach is to seek the minimum value of chi-squared,

$$(4.2) \quad \chi^2 = \sum_{i=1}^n W_i \cdot (y_i - f_i)^2$$

where the residuals are weighted by W_i . Although the principles behind HOMER and TROY are the same, their implementation is different. HOMER allows at most three exponential terms in the fitting function, while TROY allows up to 13 parameters in the fitting function, i.e. six exponential terms and a constant. On the other hand, HOMER is easier to use, because this program can find its own initial values for the fitting, while TROY requires good initial estimates to be provided. In this work, HOMER was used for the initial analysis of all the intensity decay curves, while TROY was used for the subsequent more detailed analysis, particularly cases requiring fitting functions containing more than six parameters.

Another characteristic of TROY is that it offers the possibility of fixing any combination of parameters at their initial values. In this work, TROY was used to give such constrained fits for resonance transitions for which estimates of the lifetimes of important cascades were known from theory or measurement. Lifetime components were fixed at these values while the primary lifetime and all the amplitudes were free to vary.

4.2 The ANDC Technique

As this technique uses Arbitrarily Normalized Decay Curves, it has come to be known as the ANDC method. It was initially suggested by Curtis et al. (CBB70) as a way to rigorously correct for the effects of cascading in beam-foil lifetime measurements. As mentioned in Chapter 1, this method has been used by many workers since 1971 to obtain cascade-corrected lifetimes. The basic idea is to measure intensity decay curves for the transitions that cascade directly into the primary level of interest, and then use these curves to represent the repopulation effect. The rate of change of the population of the primary level repopulated by m direct cascades given by

$$(4.3) \quad \frac{dN_k}{dt} = \sum_{j=1}^m A_{jk} N_j - N_k(t)/T_k$$

where the N_j s are the populations of the direct cascade

levels, N_k is the population of the primary level, the A_{jk} s are the Einstein transition probabilities for spontaneous emission from the j level down to the primary level, and T_k is the primary lifetime (Fig. 4.1). Using the relation between population, the corresponding intensity and S_{jk} , the relative efficiency of the detection system at wavelength λ_{jk} corresponding to the transition $j \rightarrow k$,

$$(4.4) \quad I_{jk}(t) = N_j(t) \cdot S_{jk} \cdot G \cdot A_{jk}$$

where G is a parameter depending on the geometry of the detection system, equation (4.3) can be written in the form,

$$(4.5) \quad dI_k(t)/dt = -I_k(t)/T_k + \sum_{j=1}^m I_{jk} \cdot \xi_j$$

where

$$(4.6) \quad \xi_j = A_{kn} \cdot (S_{kn}/S_{jk})$$

thus involves the ratio of detector sensitivities at the j th cascade and primary transition wavelengths. Equation (4.5) can also be written in an integral form by integrating both sides of (4.5) over the time interval t_1 to t_2 ,

$$(4.7) \quad I_k(t_2) - I_k(t_1) = (-1/T_k) \int_{t_1}^{t_2} I_k(t) dt + \sum_{j=1}^n \xi_j \int_{t_1}^{t_2} I_j(t) dt$$

All quantities (other than T_k and the ξ_j s) in equations (4.5) and (4.7) can be determined from the decay curves. T_k and the ξ_j s may then be found by fitting the expression

given by equations (4.5) and (4.7) to the observed data.

Over the years, several different techniques for applying the basic ANDC principle have been reported. In this work, two programs (ANDC and CANDY) were employed. ANDC (PGOK79) uses the integral form, equation (4.7) (Fig. 4.2). The raw data sets are used directly to calculate the integrals. The left hand side of equation (4.7) contains the difference of two intensities, which can be similar in value, and hence the difference will be very sensitive to the Poisson fluctuations. Some kind of data smoothing is therefore used to calculate this difference. In ANDC, exponential functions are fitted to sets of 5 individual data points in determining $I_k(t_1)$ and $I_k(t_2)$. A second routine CANDY (En82), uses the parameters obtained from m-e fitting to represent the smoothed data sets for the cascades. CANDY also contains sub-routines using both equation (4.5) and (4.7). If the m-e fits used to smooth the data are accurate representations of the decay data sets, CANDY should yield the more reliable result since the smoothing function has the more appropriate form. However, it is not always possible to obtain a completely satisfactory m-e fit, and an incorrect form of the m-e fitting function will distort the ANDC analysis. In such a case it is not easy to decide whether CANDY or ANDC offers the better results. Certainly the section by section smoothing used in ANDC has the advantage that the effects of a bad data point are localized to a particular panel and do

not distort the overall analysis, as may happen using the global smoothing in CANDY. In any case, consistency between the results from these two different types of analysis is a necessary test of the validity of the result.

4.3 The VNET Technique

As long ago as 1973 Irwin et al. (ILK73) demonstrated that the variation in spatial resolution at the location of the ion beam is produced by changing the spectrometer parameters (Section 2.3). If the distance between the ion beam and the spectrometer entrance slit is fixed, the spatial resolution depends on the width of the slit and grating mask employed (Fig. 2.2). Because of the vignetting problem, small values for the slit width and mask are required if it is desired to have the decay start close to the foil. This is particularly important for short-lived levels, when the most important information comes from the first few points downstream from the foil. In this work, a mean life of 40ps corresponds to a distance of 0.11mm, which was approximately two steps. However, the minimum practical width of the slit and mask are limited by the weakness of the beam-foil light source. To make full use of the information contained in the first few downstream points, it is desirable to include some of the points in the vignetting region. To achieve this, it is necessary to use a more

FIGURE 4.1

Representative Energy Level Scheme

Showing the repopulation of the primary level K by several cascade levels, J . Here N_J represents the populations of the J levels.

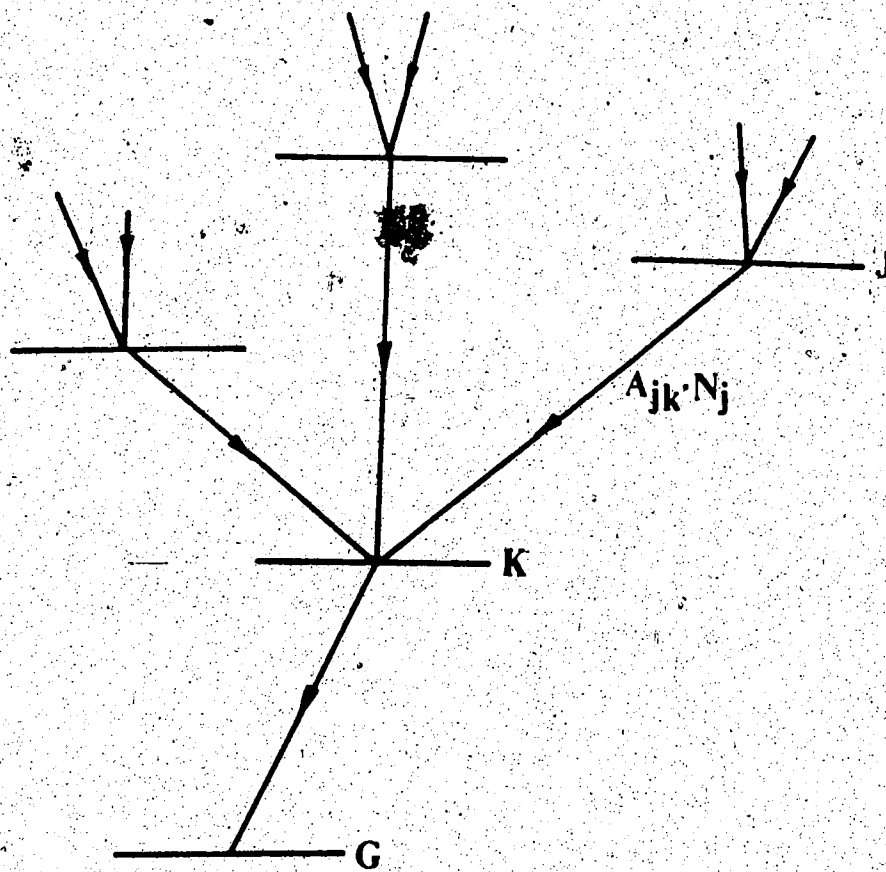


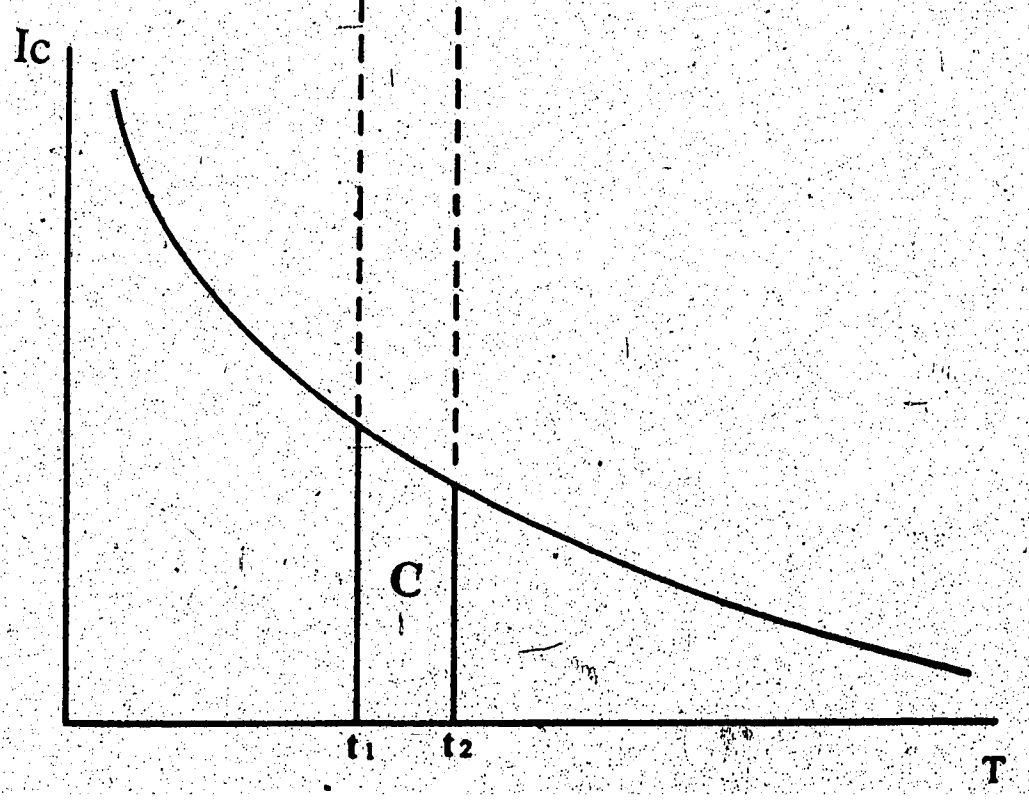
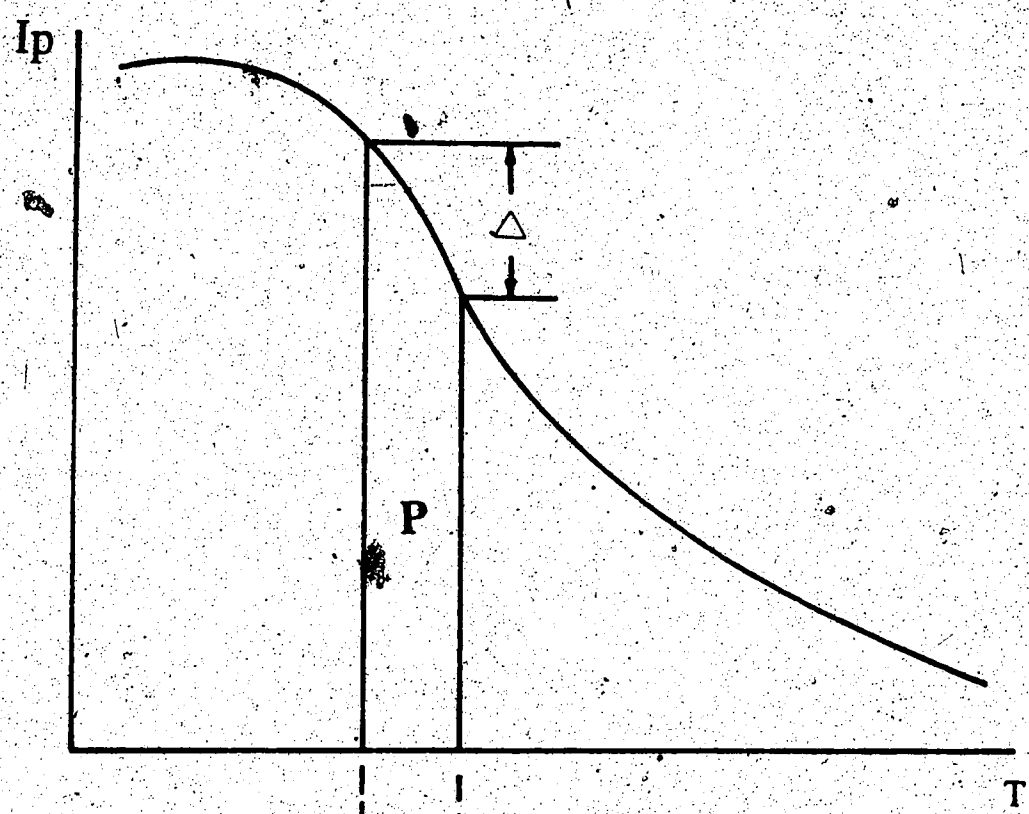
FIGURE 4.2

Schematic Decay Curve Used In An RNDG Analysis

Showing the quantities P, C and Δ that are fitted to equation 4.7, where

$$P = \int_{t_1}^{t_2} I_k(t) dt, \quad C = \int_{t_1}^{t_2} I_l(t) dt, \quad \text{and}$$

$$\Delta = I_k(t_2) - I_k(t_1)$$



complicated fitting routine which considers the vignetting effect.

It is easy to see that, although the observed intensity is the convolution of the true spatial distribution of the decaying signal and the window function, the lifetimes themselves will generally not be affected if only points from outside the vignetting region are involved in the analysis. The true intensity decay downstream from the foil, may be written as a sum of exponentials i.e.

$$(4.8) \quad \begin{aligned} I(t) &= 0 & t < 0 \\ I(t) &= \sum_{i=1}^m C_i \cdot \exp(-t/T_i) & t \geq 0 \end{aligned}$$

where the C_i are constants depending on the initial populations and the Einstein transition probabilities of the levels involved, and t is the time duration for the ion beam travelling from the foil to the given position. Similarly, the spatial resolution at the ion beam can be represented by a window function of t' ,

$$(4.9) \quad \begin{aligned} W(t') &= 0 & t' < a \\ & & \text{or } t' > b \\ W(t') &= \text{any appropriate function} & a \leq t' \leq b \end{aligned}$$

where t' is the time duration for the ion beam travelling from a point on the optical axis of the detection system to a particular position. Combining equations 4.8 and 4.9, the observed intensity may be written as

$$I_0 = \int_{-\infty}^{\infty} W(t') \cdot I(t+t') dt' \quad (4.10)$$

$$= \sum_{i=1}^m C_i \exp(-t/T_i)$$

where

$$(4.11) \quad C_i = \int_{-\infty}^{\infty} C_i \cdot W(t') \exp(-v \cdot t'/T_i) dt$$

From equation 4.10 and 4.11, the amplitudes of the terms will be distorted by the window, but the lifetimes remain unchanged. This is only the case without vignetting.

In the vignetting region, the calculation is more complicated. The integrand in equation 4.10 is changed, since there is no radiation emitted from the upstream side of the foil. In other words, the window is effectively truncated at the foil. Instead of being a constant as shown in equation 4.11, the coefficient will now be a function of t , i.e.

$$(4.12) \quad C_i' = \int_{-\infty}^{\infty} C_i \cdot W(t') \exp(-t'/T_i) dt$$

Comparing equations 4.11 and 4.12, it is clear that a correction is required in calculating the amplitudes in the vignetting region.

A program called VNET has been written locally (W.Ansbacher, private communication) to include the truncation effect in the vignetting region. A standard

trapezoid was used to represent the window function (Fig. 2.2). The fitting procedure is based on the same algorithm TROY, but includes 4 additional fitting parameters; 3 for the shape of the window and one for the position of the foil. The method of execution in VNET is essentially the same as that used in TROY.

In this work, the experiment employed a small distance (2.0cm) between the ion beam and the entrance slit. Consequently, the size of the window was small, and only a few (typically 4) points are involved in the vignetting region. It is not surprising that VNET generally yielded results that were not significantly different from HOMER/TROY. The only case for which VNET analysis gave somewhat different results were those involving very short-lived energy levels.

5. LIFETIME MEASUREMENTS

The results of analyses using the techniques introduced in Chapter 4 will be discussed in this chapter. Free m-e techniques (HOMER/TROY and VNET) were used to analyze the lifetimes for the cascade levels. The results are discussed in Section 5.1, where they are compared with the theoretical values. Lifetimes for the resonance levels were obtained using free multi-exponential fitting, constrained fitting and the ANDC techniques. These results are discussed in Section 5.2 where the measured lifetimes are compared with previous experiments and the theoretical predictions.

5.1 Lifetimes of Levels of the $3p^2$ and $3s3p3d$ Configuration

Decay curves were measured for 15 lines assigned as transitions from the $3p^2$ or $3s3p3d$ down to $3s3p^2$ or $3s^23d$ levels. Free multi-exponential fitting analysis and VNET analysis were employed for these decay curves. The results are shown in Table 5.1. Comparing the results from the free multi-exponential analysis and the theoretical prediction, the measured lifetimes are seen to be typically 30% longer than theory, the discrepancies tending to be larger for the shorter-lived levels. As discussed in Section 4.2, a lifetime of 40ps corresponded approximately to 2 steps in this work. Furthermore, the first four points downstream from the foil were usually truncated as they fell in the

vignetting region discussed in Section 4.3. Measurements made using an observation window that is comparable to, or even longer than the primary decay length (i.e. the distance along the beam corresponding to one lifetime of the primary level) is known (OPDB79) to give a significantly reduced amplitude to the coefficient of the primary lifetime term, and hence such short lifetimes become difficult to measure accurately. Of course, cascade effects may also be involved in lengthening the measured values of the primary lifetimes. It is worth noting that VNET yielded somewhat better agreement with the theoretical values for three very short-lived levels, $3s3p(^3P)3d\ ^3D$ ($J=5/2$), 3F ($J=7/2$) and $3s3p(^1P)3d\ ^3P$ ($J=1/2$). On the other hand, the theoretical values may well be too short, because mixing with higher levels (not included in the theoretical calculations) would tend to transfer line-strength from the transitions measured here to transitions from those higher levels, and hence increase the lifetimes of the $3p^2$ and $3s3p3d$ levels (B.C. Fawcett, private communication).

5.2 Lifetimes of the $3s3p^2$ and $3s^23d$ Energy Levels

Decay curves were measured for eight resonance lines. The various techniques (HOMER/TROY, VNET, ANDC) described in Chapter 4 were employed to analyze these data. The results of these analyses are shown in Table 5.2. The free

Table 5.1

Radiative Lifetimes of $3p^3$ and $3s3p3d$ Levels of Ar VI

LEVEL			LIFETIME (NS)		
Term	J		TROY ^a	VNET ^b	Theory ^c
$3p^3$	2P	1/2	0.25 ± 0.03	0.26 ± 0.04	0.18
		3/2	0.23 ± 0.03	0.26 ± 0.04	0.18
	2D	3/2	1.31 ± 0.10	1.31 ± 0.10	1.07
		5/2	1.24 ± 0.08	1.30 ± 0.08	1.04
$3s3p(^3P)3d$	2P	1/2	0.067 ± 0.006	0.075 ± 0.007	0.052
		3/2	0.072 ± 0.007	0.070 ± 0.008	0.050
	2D	3/2, 5/2	0.081 ± 0.008	0.088 ± 0.005	0.068
	2F	5/2	0.14 ± 0.02	0.13 ± 0.02	0.13
		7/2	0.13 ± 0.02	0.13 ± 0.02	0.12
$3s3p(^1P)3d$	2P	1/2	0.065 ± 0.018	0.046 ± 0.015	0.029
	2D	5/2	0.061 ± 0.018	0.040 ± 0.010	0.029
	2F	7/2	0.086 ± 0.020	0.055 ± 0.010	0.049

a. Multi-exponential curve fitting result.

b. Multi-exponential curve fitting result incorporating a window function and including the region containing the foil (see text).

c. Configuration-interaction calculation using scaled Slater integrals. (Fa83)

Multi-exponential techniques yielded somewhat longer lifetimes than the other analyses, especially for the short-lived energy levels. (The difficulties associated with measuring short lifetimes were discussed in Section 5.1). Since the lifetimes of the resonance energy levels correspond to distances along the beam that are longer than both the observation window and the separation of the measured points, the VNET values were not significantly different from the HOMER/TROY results. On the other hand, the ANDC analysis gave significantly shorter lifetimes than the other analyses for the short-lived levels. In the case of the $3s3p^2 \ ^2D$ levels, where the primary lifetimes are much longer than that of any important cascades, little variation in the lifetimes is observed from one method of analysis to another. The ANDC analysis for the individual levels will now be discussed in turn.

5.2.1 $3s3p^2 \ ^2S$

Fawcett's calculation suggested that the most important cascade into $3s3p^2 \ ^2S$ levels should be from the $3s3p(^2P)3d \ ^2P$ levels and this is supported by the observed spectra, where the transitions from $3p^3 \ ^2P$ and $3s3p(^2P)3d \ ^2P$ are found to be very weak. In Table 5.2, it may be seen that the ANDC analysis gives significantly closer agreement with the theoretical value.

5.2.2 $3s3p^2 \ ^2P$

Fawcett's calculation predicted that several cascades may be involved significantly in the repopulation of the $3s3p^2 \ ^2P$ levels. The relative intensities of the observed spectrum lines indicate that the transitions from the $3p^3 \ ^2P$ ($J=1/2$), 2D ($J=5/2$), $3s3p(^2P)3d \ ^2P$ ($J=1/2$) and $3s3p(^1P)3d \ ^2P$ levels are important cascades for the repopulation of the $3s3p^2 \ ^2P$ ($J=1/2$) level. Since the $3p^3 \ ^2D$ levels have much longer lifetimes than does the primary level, $3s3p^2 \ ^2P$ ($J=1/2$), only the 2P levels of the $3p^3$, $3s3p(^2P)3d$ and $3s3p(^1P)3d$ were selected as cascades in the ANDC analyses for $3s3p^2 \ ^2P$ ($J=1/2$). The theoretical predictions also suggest that an even greater number of energy levels is involved in repopulating the $3s3p^2 \ ^2P$ ($J=3/2$) level. ANDC analyses for this level were attempted using both three cascades (from $3s3p(^2P)3d \ ^2P$, $3s3p(^1P)3d \ ^2P$ and 2D) and four cascades (from $3s3p(^2P)3d \ ^2P$, $3s3p(^1P)3d \ ^2P$, 2D and $3p^3 \ ^2P$). Since the decay curves measured at 468, 469, 497 and 502 Å appear very similar, no distinction was made between these two $3s3p(^1P)3d \ ^2P$ levels in the ANDC analyses. The ANDC analyses did not appear to be sensitive to the cascade level $3p^3 \ ^2P$, which has a relatively long lifetime among these cascade levels. Although the ANDC analyses give closer agreement with theory than do the other methods for $3s3p^2 \ ^2P$ ($J=3/2$), this agreement is relatively poor compared to those for the other resonance levels. This may indicate that problems can occur for ANDC analyses involving a large

number of important cascades.

5.2.3 $3s3p^2 \ ^2D$

These levels have much longer lifetimes than any of the cascades. Transitions from the $3p^2 \ ^2P$ and 2D levels were chosen as the important cascades for these levels, since they are the only intense cascades with relatively long lifetimes. The lifetimes obtained for these levels were relatively insensitive to the form of analysis used.

5.2.4 $3s^23d \ ^2D$

For the $3s^23d \ ^2D$ ($J=3/2$) level, the $3s3p(^2P)3d \ ^2F$, $3s3p(^2P)3d \ ^2P$ and 2F were chosen as the important cascade levels, while for the ($J=5/2$) level, the $3s3p(^2P)3d \ ^2F$ and $3s3p(^2P)3d \ ^2D$ and 2P levels were used. The ANDC results were found to show significantly closer agreement with theory than the results from other methods of analysis. It was mentioned in Chapter 3 that the assignment of the $3s3p(^2P)3d \ ^2F$ (and to a lesser extent 2D) levels are still somewhat tentative. The error estimates for these two levels have therefore been increased in Table 5.2 to allow for these factors.

5.3 Discussion of Lifetime Results

It is interesting to compare the ANDC results for the resonance levels in this work with those in the recent study

of TiX. There are some similarities in these two works. First of all, the ANDC analysis yields shorter lifetimes, and gives closer agreement with theoretical calculation than the free m-e technique in both works for the resonance levels, especially for the short-lived $3s3p^2\ ^2S$, 2P and $3s^23d\ ^2D$ levels. Secondly, the ANDC results for $3s3p^2\ ^2P$ ($J=3/2$) in this work still show relatively bigger discrepancies with theoretical values than for the other resonance levels, and the study of TiX shows similar results. It was suggested (PAHH87) that the problem may be a combination of the rather large but weak number of cascades that must be considered in the ANDC analyses for the $3s3p^2\ ^2P$ levels and the short lifetimes of the levels involved.

Constrained multi-exponential fitting was also applied for the resonance levels by using TROY with the important cascade lifetimes fixed at the theoretical or the measured values, and other parameters free to vary. The results were generally in agreement with the ANDC results within the uncertainties obtained from these analyses. For the $3s3p^2\ ^2S$ levels, the main cascade levels are expected to be the $3s3p(^2P)3d\ ^2P$ and $3s3p(^1P)3d\ ^2P$ levels. Therefore two cascade lifetimes were fixed at 0.070 and 0.050ns to represent these cascade levels in a TROY 5-term fit. For the $3s3p^2\ ^2P$ levels, three cascade lifetimes of 0.050, 0.21 and 1.25ns were fixed to represent the cascade levels in a TROY 5-term fit. The lifetime of 0.050ns represented the short-lived $3s3p(^2P)3d\ ^2P$ and $3s3p(^1P)3d\ ^2P$, 2D levels while

0.21 and 1.25ns represented the $3p^2\ ^2P$ and 2D levels respectively. For the $3s3p^2\ ^2D$ levels, three lifetimes fixed at 1.25, 0.21 and 0.12ns were used in a TROY 6-term fit to represent the cascade levels, $3p^2\ ^2D$, 2P and $3s3p^2\ ^2P$ respectively. For the $3s^23d\ ^2D$ levels, the important cascades are expected to be from the $3s3p(^2P)3d\ ^2F$ and $3s3p(^2P)3d$ levels. Since the $3s3p(^2P)3d$ levels have lifetimes very close to those of the $3s^23d$ levels, it is not possible to separate these components in a constrained m-e fit. Hence, only one fixed lifetime parameter was included to represent the $3s3p(^2P)3d\ ^2F$ levels in a TROY 4-term fit. The results of the constrained fitting are shown in Table 5.2. All the results seem generally in good agreement with those of the ANDC method within the uncertainties.

Comparing the present results with those from previous experiments (LPIK81, BBC82), good agreement is found for the long-lived $3s3p^2\ ^2D$ levels, but the present results show closer accord with Fawcett's calculations for the $3s3p^2\ ^2S$ and $3s^23d\ ^2D$ levels (Table 5.3). On the other hand, the earlier results obtained by Buchet-Poulizac et al. agreed well with Fawcett's values for the $3s3p^2\ ^2P$ levels, even though no rigorous cascade correction was applied in their experiment.

Radiative Lifetimes of 3s3p¹ and 3s²3d Levels of ArVI

LIFELIMES^c (NS)

LEVEL	J	TROY	VNET	Constrained	ANDC	Theory ^a
3s3p ¹ 'S	1/2	0.260 ± 0.029	0.262 ± 0.022	0.245 ± 0.025	0.227 ± 0.010 ^b	0.22
'P	1/2	0.104 ± 0.006	0.097 ± 0.006	0.110 ± 0.030	0.074 ± 0.005 ^c	0.069
	3/2	0.099 ± 0.005	0.101 ± 0.005	0.078 ± 0.020	0.084 ± 0.010 ^d	0.068
'D	3/2	2.38 ± 0.08	2.13 ± 0.20	2.14 ± 0.20	2.14 ± 0.10 ^e	2.3
	5/2	2.58 ± 0.08	2.23 ± 0.20	2.23 ± 0.20	2.29 ± 0.10 ^e	2.4
3s ² 3d 'D	3/2	0.090 ± 0.010	0.080 ± 0.005	0.053 ± 0.012	0.060 ± 0.015 ^f	0.057
	5/2	0.094 ± 0.012	0.104 ± 0.005	0.061 ± 0.014	0.060 ± 0.015 ^f	0.058

a. Configuration-interaction calculation using scaled Slater integrals (Fa83)

b. Analyses incorporating cascade data from 3s3p('P)3d¹'P.

c. Analyses incorporating cascade data from 'P levels of 3s3p('P)3d, 3s3p('P)3d and 3p¹, the 'D levels of 3s3p('P)3d.

d. Analyses incorporating cascade data from 3s3p('P)3d 'P, 3s3p('P)3d 'P and 3p¹'P

e. Analyses incorporating cascade data from 3p¹'P and 'D.

f. Analyses incorporating cascade data from 3s3p('P)3d 'F, 3s3p('P)3d 'D and 'F.

Table 5.3

Comparison With Previous Experiments

LEVEL		LIFETIME (NS)		
Term	J	This Work (ANDC)	Other Exp.	Theory ^a
3s3p ²	² S 1/2	0.227 ± 0.010	0.29 ± 0.03 ^b	0.22
			0.27 ± 0.03 ^c	
	² P 1/2	0.074 ± 0.005	0.069 ± 0.07 ^b	0.069
			0.072 ± 0.07 ^b	
	3/2	0.084 ± 0.012	0.10 ± 0.01 ^c	0.068
² D	3/2	2.14 ± 0.10	2.40 ± 0.20 ^b	2.3
	5/2	2.29 ± 0.10	2.48 ± 0.20 ^b	2.4
			2.4 ± 0.2 ^c	
3s ² 3d	² D 3/2	0.060 ± 0.015	0.085 ± 0.009 ^b	0.057
			0.087 ± 0.009 ^b	
	5/2	0.060 ± 0.015	0.08 ± 0.02 ^c	0.058

a. Configuration-interaction calculation using scaled Slater integrals (Fa83).

b. Earlier beam-foil results using m-e curve fitting (BBC82).

c. Earlier beam-foil results using m-e curve fitting (LPI81).

6. SUMMARY AND CONCLUSIONS

The beam-foil spectrum of ArVI in the ($n=3$) array has been studied. Several different methods have been used to suggest assignments for energy levels of the $3p^3$ and $3s3p3d$ configurations. Comparison of experimental and theoretical data for other ions in the AlI isoelectronic sequence was first used to provide estimates of the energies of the $3p^3$ and $3s3p3d$ levels. A computer program was then used to search the observed spectrum for transitions between these energy levels and the $3s3p^2$ and $3s^23d$ levels. Two different approaches were then used to analyze the decay curves recorded for the assigned transitions from these $3p^3$ and $3s3p3d$ levels, namely multi-exponential fitting procedures (HOMER/TROY/VNET) and comparison of the shapes of the intensity decay curves for transitions from the same upper level (TFIT). Finally, the relative intensities of transitions from the upper term were studied and compared with the theoretical predictions. As a result, 30 transitions were assigned involving 15 levels of $3p^3$ and $3s3p3d$ electron configurations.

Previous assignments for the $3s3p3d$ 3P and 3D levels suggested by Buchet-Poulizac et al. have been reassigned as $3p^3$ levels on the basis of isoelectronic sequence trends. Further support for this revision was obtained from spectroscopic and intensity decay curve analyses. The same techniques were also applied to assign the $3s3p(^3P)3d$

levels. Good evidence was found for the assignments of the $3s3p(^3P)3d\ ^3P$, 3D and 3F levels. It has to be mentioned that the $3s3p(^1P)3d$ levels were only tentatively assigned because the TFIT analysis did not yield consistent results for transitions from 3F , and it was only possible to record one decay curve for a single transition from both 3P and 3D . Finally, the fact that ANDC analysis for the resonance levels was successful when incorporating the transitions assigned for the $3p'$ and $3s3p3d$ levels as cascades also provides some support for these assignments.

Comparisons between the observed results and Fawcett's predictions (Table 6.1) show many similarities to those in the study of isoelectronic element, TiX (PATH87). It is interesting to note that the theoretical calculations correctly predicted all the inverted doublets in the $3p'$ and $3s3p3d$ configurations. The weighted mean of the ratio of the measured to Fawcett's calculated cascade lifetimes is 1.25. Apart from this systematic deviation, the experimental results show a generally good qualitative correspondence with the theoretical calculations. The cascade lifetimes measured in TiX show a similar trend. Although Huang's calculation is not so complete, it is interesting that the overall agreement for the cascade lifetimes is somewhat better in ArVI.

In the studies of ArVI and TiX, the ANDC analyses yielded primary lifetimes very close to the theoretical values for most cases. The agreement between the ANDC

results and theory implies that the ANDC technique is still a useful and powerful tool in atomic systems having three active electrons. In this work, the selection of important cascades relied on the theoretical predictions and the spectroscopic intensities of these cascading transitions. One fact must be borne in mind when selecting cascades. Since configuration-interaction varies along an isoelectronic sequence, the major cascades for the same primary level may be different from one element to another in the same sequence. For example, the $3s3p(^1P)3d\ ^3D$ levels are major cascade levels for the $3s^23d\ ^3D\ (J=3/2)$ level in TiX, but not in ArVI. The common problem met in ArVI and TiX during the ANDC analyses is the difficulty in obtaining a satisfactory result for the $3s3p^2\ ^3P$ levels. As was discussed in Chapter 5, the combination of a large number of cascades and the short primary lifetimes might be part of the reason for this difficulty. The degree of difficulty found in applying the ANDC method to systems having three active electrons is significantly greater than has been found previously for system having one or two active electrons. This suggests that applying the ANDC technique to four-electron systems will not be an easy task.

Table 6.1

Comparison With Calculations*

Ratio of Observed Value/Fawcett's Value

<u>QUANTITY</u>	<u>ARVI</u>	<u>TIX</u>
Level Energies	0.988 (0.006)	0.990 (0.008)
Doublet Splittings	1.05 (0.25)	0.89 (0.15)
Cascade Lifetimes	1.25 (0.10)	1.28 (0.14)
Primary Lifetimes	0.99 (0.06)	0.98 (0.06)

Ratio of Observed Value/Huang's Value

<u>QUANTITY</u>	<u>ARVI</u>	<u>TIX</u>
Level Energies	0.990 (0.010)	0.991 (0.007)
Doublet Splittings	0.95 (0.35)	0.98 (0.54)
Cascade Lifetimes**	1.08 (0.12)	1.27 (0.20)
Primary Lifetimes	1.00 (0.09)*	1.00 (0.06)

- * The value in brackets represents the r.m.s. deviation.
- ** Levels with j value less than $5/2$ are not included since f values for these levels are not available in Huang's calculation. The corresponding observed/Fawcett values using only these transitions are 1.18(0.07) and 1.25(0.11) for ArVI and TiX respectively.

BIBLIOGRAPHY

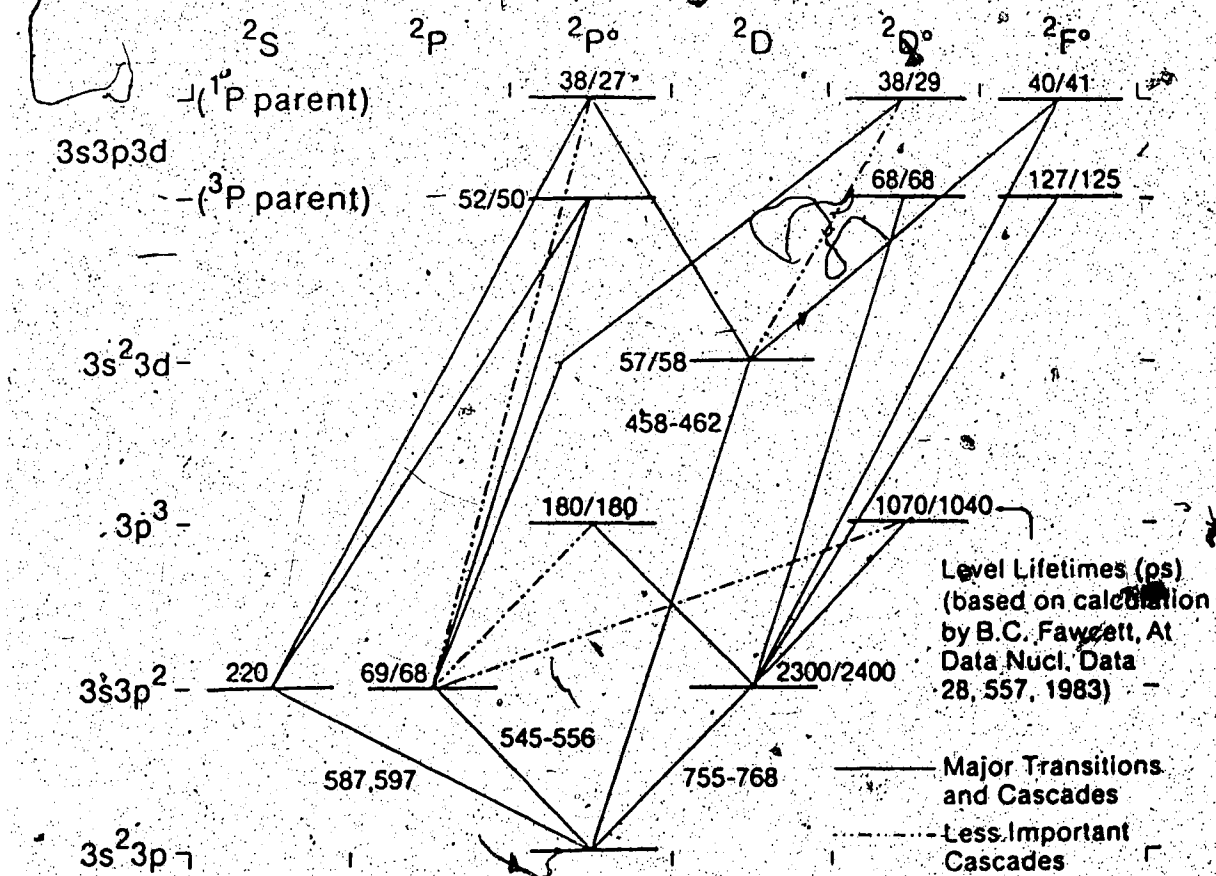
- AUT84. K. Aashamar, T.M. Luke and J.D. Talman, *Physica Scripta* 30, 121 (1984).
- Ba64. S. Bashkin, *Nucl. Instr. & Meth.* 28, 88 (1964).
- BBC82. M.C. Buchet-Poulizac, J.P. Buchet and P. Ceyzeriat, *Nucl. Instr. and Meth.* 202, 13 (1982).
- BBL73. S. Bashkin, J. Bromander and J. Martinson, *Physica Scripta* 8, 285 (1973).
- BDG82. Y. Baudinet, P.D. Dumont and H.P. Garnir, *Nucl. Instr. and Meth.* 202, 33 (1982).
- Be69. P.R. Bevington, 37, "Data Reduction and Error Analysis for the Physical Sciences", McGraw Hill, New York.
- BGDL76. Y. Baudinet-Robinet, H.P. Garnir, P.D. Dumont and A.E. Livingston, *Physica Scripta* 14, 224 (1976).
- BM71. S. Bashkin and I. Martinson, *J. Opt. Soc. Am.* 61, 1686 (1971).
- BPK082. J.L. Bahr, E.H. Pinnington, J.A. Kernahan and J.A. O'Neill, *Can. J. Phys.* 60, 1108 (1982).
- CBB70. L.J. Curtis, H.G. Berry and J. Bromander, *Phys. Rev.* 2, 216 (1970).
- Ed63. B. Edlén, "Report On Progress In Physics", 26, 181 (1963).
- EEB83. J.O. Ekberg, L. Engström, S. Bashkin, B. Denne, S. Hultet, S. Johansson, C. Jupén, U. Litzen, A. Trigueiros and I. Martinson, *Physica Scripta* 27, 425 (1983).
- En82. L. Engström, *Nucl. Instr. and Meth.* 202, 369 (1982).
- Fa83. B.C. Fawcett, *Atom. Data Nucl. Data Tab.* 28, 557 (1983).
- FTW61. B.C. Fawcett, B.B. Jones and R. Wilson, *Proc. Phys. Soc.* 78, 1223 (1961).
- Fi81. C.F. Fischer, *Physica Scripta* 23, 38 (1981).
- Hu86. K.N. Huang, *Atom. Data Nucl. Data Tab.* 34, 1 (1986).

Table A4.1
Theoretical Calculation of A-values (10^{-9} s⁻¹) and Lifetimes (ps)
For 3p, and 3s3p3d Levels

Upper level	Lower level		3s ² 3d		3s3p ²			T(ps)
			3/2	5/2	3/2	5/2	1/2	
3p ²	¹ P (J=1/2)		----	----	4.30	----	0.672	180
	³ P (J=3/2)		----	----	0.398	3.79	0.096	180
	¹ D (J=3/2)		----	----	0.662	0.421	0.133	1070
	³ D (J=5/2)		----	----	0.058	0.750	0.151	1040
3s3p(1P)3d	¹ P (J=1/2)		----	----	----	----	5.47	52
	³ P (J=3/2)		0.026	0.014	----	----	0.998	50
	¹ D (J=3/2)		0.074	----	12.9	1.29	0.354	68
	³ D (J=5/2)		----	0.074	1.03	13.2	0.378	68
3s3p(1P)3d	¹ F (J=5/2)		0.481	0.048	6.74	0.579	----	127
	³ F (J=7/2)		----	0.549	7.47	----	----	125
3s3p(1P)3d	¹ P (J=1/2)		14.6	----	----	----	5.80	38
	³ P (J=3/2)		8.14	1.84	----	0.001	19.8	27
	¹ D (J=3/2)		0.816	14.0	0.106	----	3.69	38
	³ D (J=5/2)		0.373	7.69	----	----	26.6	29
3s3p(1P)3d	¹ F (J=5/2)		10.8	0.654	12.4	0.885	----	40
	³ F (J=7/2)		----	11.3	13.3	----	----	41

FIGURE A4.1

Energy Level Scheme of ArVI ($n=3$)



APPENDIX V SAMPLE LIFETIME ANALYSES

Fig. A5.1(a) - Fig. A5.1(d) show examples of lifetime analyses for data recorded at 462.0A for the transition from $3s^2 3d^2 D$ ($J=5/2$) down to $3s 3p^2 P$ ($J=3/2$). Four techniques are illustrated :

TROY (free fitting) Fig. A5.1(a)

VNET Fig. A5.1(b)

TROY (constrained fitting) Fig. A5.1(c)

ANDC Fig. A5.1(d)

The data to be analyzed were recorded from 0.1mm to 8mm downstream from the foil. In the TROY (free fitting) analysis with six fitted parameters shown in Fig. A5.1(a), the first three data points are truncated to avoid the vignetting region, since the viewing length is about 0.4mm. In the VNET analysis shown in Fig. A5.1(b), four extra fitted parameters are introduced, one for the foil position and three for the viewing window, to include the data points in the vignetting region, and hence no data points are truncated in this analysis. As may be seen from the analysis, the primary lifetime so derived is not significantly different from that obtained using a free TROY fit. In the constrained TROY analysis with seven parameters shown in Fig. A5.1(c), one cascade lifetime is fixed at 0.125ns to represent the cascading effect from the $3s 3p(^1P) 3d^2 F$ ($J=7/2$) level. The primary lifetime is found to be 0.0591 ± 0.0146 ns, which is in good agreement with the theoretical prediction (Table A4.1). In the ANDC analysis shown in Fig. A5.1(d), the three

transitions at 472.1, 594.8 and 470.9 Å are used to represent the important cascade levels: $3s3p(^1P)3d\ ^1D$, 1F and $3s3p(^1P)3d\ ^3F$. The fit looks reasonable, as judged by the chi-squared value being close to unity and the random appearance of the scatter plot. The probe value is defined (equation 4.5-4.7) as the transition probability for the primary transition multiplied by the ratio of the sensitivities of the detection system at the primary and cascade wavelengths. If this ratio is unity, the observed primary lifetime (0.061 ns) suggested that a probe value of around 16 should be expected. This is consistent with the observed values for the second and third cascades. In the case of the 472.1 Å cascade, this is in fact the strongest branch from the $3s3p(^1P)3d\ ^1D$ term, the actual transition to $3s\ ^1D$ ($J=5/2$) lying at 574 Å. This effectively increases the detector sensitivity by a factor of three, thus giving a proportionally lower probe value, as found in the analysis. Of course, a minimum requirement for the probe values is that they all be positive, as is the case here.

N.B. Each example shown in Fig. A5.1 represents one run using a given technique. The final results quoted in Table 5.2 are weighted means of the values obtained from several different runs.

FIGURE A5.1

Sample Lifetime Analyses

A5.1(a) TROY(free fitting)

A5.1(b) VNET

A5.1(c) TROY(constrained fitting)

A5.1(d) ANDC

[illegible]

SOURCE	MV	LAMDA	#	CHISO/DEC FR	MM/MS	MAR 30 1988	# 62212
ARSS	1.5	482	5	1.083	2.745		
PARAMETER'S	A	TA(NS)	B	TR(NS)	C	TC(NS)	D
VALUE	8225.50	0.1045	515.78	0.4244	72.88	3.5185	
STD DEV	145.71	0.0033	142.27	0.0635	56.83	2.6682	
PER CENT	1.5	3.2	17.4	22.0	78.0	106.8	
WARP FACTORS		1.0409		1.0025		1.0000	
WINDOW PARAMETERS							
VALUE	SIZE(DMM)	H WIDTH(MM)	WID(MM)	SLOPE(%)			
STD DEV	2.11	0.100	0.200	20.000			
	0.004	0.0	0.0	0.0			
CHISO	#DEC FR	#PARS	#TEAMS	FITTED	REJECTED	TRUNCATED	
46.57	43	10	7	50	0	0	
V111	T111	V111-BKG			V111		DIV/SIC PLOT
M.M	SEC	DATA	CALC	(DV/SIC)	DATA	CALC	0.0
6.30	28.0	5274.0	5271.2	0.03	5274	5271.2	
6.35	27.8	5275.0	5235.2	-1.80	5275	5435.2	
6.40	28.1	5083.0	5019.2	0.53	5083	5019.2	
6.45	28.7	4411.0	4322.8	1.15	4411	4322.8	
6.50	28.4	3854.0	3722.8	2.00	3854	3722.8	
6.55	27.8	3257.0	3215.2	0.85	3257	3215.2	
6.60	28.2	2721.0	2785.2	-1.11	2721	2785.2	
6.65	27.7	2375.0	2420.7	-0.85	2375	2420.7	
6.70	28.4	2070.0	2111.8	-0.83	2070	2111.8	
6.75	28.6	1870.0	1848.8	0.45	1870	1848.8	
6.80	27.5	1804.0	1824.8	0.48	1804	1824.8	
6.85	28.1	1475.0	1434.3	0.85	1475	1434.3	
6.90	27.9	1247.0	1271.8	-0.65	1247	1271.8	
6.95	28.5	1115.0	1132.5	-0.48	1115	1132.5	
7.00	28.7	1008.0	1013.3	-0.16	1008	1013.3	
7.05	28.5	825.0	810.8	0.44	825	810.8	
7.10	28.5	830.0	822.7	0.24	830	822.7	
7.15	27.7	728.0	748.8	-0.65	728	748.8	
7.20	28.4	645.0	680.8	-1.33	645	680.8	
7.25	28.5	537.0	523.3	0.51	537	523.3	
7.30	28.1	585.0	573.4	0.88	585	573.4	
7.35	28.1	498.0	491.4	0.28	498	491.4	
7.40	28.1	446.0	427.7	0.82	446	427.7	
7.45	28.3	409.0	377.4	1.49	409	377.4	
7.50	28.5	357.0	337.0	1.01	357	337.0	
7.55	28.1	285.0	303.8	-1.01	285	303.8	
7.60	28.4	252.0	275.8	-0.85	252	275.8	
7.65	28.2	254.0	253.2	0.05	254	253.2	
7.70	28.1	235.0	233.3	0.05	235	233.3	
7.75	27.8	212.0	215.0	-0.27	212	215.0	
7.80	28.5	180.0	200.8	-1.49	180	200.8	
7.85	28.5	175.0	175.3	0.18	175	175.3	
7.90	28.2	167.0	154.8	0.81	167	154.8	
7.95	28.3	137.0	137.8	-0.05	137	137.8	
8.00	28.3	123.0	123.3	-0.03	123	123.3	
8.05	28.1	111.0	111.2	-0.02	111	111.2	
8.10	28.2	115.0	101.0	1.33	115	101.0	
8.15	28.3	85.0	92.3	0.37	85	92.3	
8.20	28.3	89.0	84.8	0.43	89	84.8	
8.25	28.0	81.0	78.3	2.13	81	78.3	
8.30	28.8	79.0	72.8	0.87	79	72.8	
8.35	28.0	82.0	83.8	-0.21	82	83.8	
8.40	27.8	85.0	85.8	1.40	85	85.8	
8.45	28.3	83.0	81.8	0.19	83	81.8	
8.50	28.1	49.0	47.3	0.82	49	47.3	
8.55	28.4	82.0	43.8	1.08	82	43.8	
8.60	28.0	28.0	41.1	2.15	28	41.1	
8.65	28.5	41.0	38.7	0.35	41	38.7	
8.70	28.5	41.0	38.8	0.85	41	38.8	
8.75	27.5	32.0	34.8	0.25	37	34.8	

Fig. A5.1(b) VNET

AR06 1.5 452.5
 AR07 1.5 472.1
 AR07 1.5 505.1
 AR07 1.5 471.1

VALID FITTED DELTA S. DEV				(FIT-DEL)/S DEV/CHISQ					AREA SD+2		AREA SD+2		AREA SD+2		AREA SD+2	
				-3	-2	-1	0	1	2	3						
0.5	1360	1360	42								181.4	2.2	21.7	0.3	17.5	0.2
0.5	883	887	30								119.1	1.6	18.7	0.2	13.7	0.2
0.5	646	655	31								88.7	1.2	14.1	0.2	10.8	0.1
0.5	485	485	27								67.4	0.9	11.0	0.1	7.8	0.1
0.5	378	387	24								52.2	0.7	9.7	0.1	6.3	0.1
1.1	259	258	21								40.8	0.6	8.8	0.1	5.2	0.1
1.1	192	188	19								33.5	0.5	7.4	0.1	4.3	0.1
2.2	115	134	17								26.8	0.4	6.6	0.1	3.8	0.1
2.2	98	101	16								22.8	0.3	5.8	0.1	3.4	0.0
1.1	152	127	14								37.1	1.0	10.1	0.3	5.0	0.1
0.8	115	109	13								28.5	0.6	8.3	0.2	4.4	0.1
1.3	98	71	11								21.7	0.5	7.3	0.2	3.9	0.1
2.0	33	49	10								18.1	0.5	6.9	0.2	2.7	0.1
4.6	22	28	9								15.1	0.4	5.6	0.2	2.2	0.1
1.3	14	42	8								25.6	1.4	8.9	0.5	3.8	0.2
2.2	22	26	8								20.5	1.1	7.8	0.4	2.3	0.1
1.8	27	23	7								18.8	0.9	6.4	0.3	1.7	0.1

LIFETIME: 0.081 0.008

PROBE: 6.6124 9.5557
 16.8678 11.8288
 30.1855 14.1592

CHISQ: 0.710

University of Alberta

Fig. A5.1(d) ANDC